Development of Printed-Circuit-Board Based Industry-Compatible Point-of-Care Biosensing and Bioprocessing Technology with Applications

by

Hsiu-Yang Tseng

M.Sc., University of Washington, 2010

Thesis Submitted in Partial Fulfillment of the
Requirements for the Degree of
Doctor of Philosophy

in the
School of Engineering Science
Faculty of Applied Sciences

SIMON FRASER UNIVERSITY

Fall 2015

Approval

Name:	**Hsiu-Yang Tseng**
Degree:	**Doctor of Philosophy**
Title:	***Development of Printed-Circuit-Board Based Industry-Compatible Point-of-Care Biosensing and Bioprocessing Technology with Applications***
Examining Committee:	**Chair:** Dr. John Jones, P. Eng. Associate Professor

Dr. Bonnie Gray, P. Eng.
Senior Supervisor
Associate Professor _____

Dr. Bozena Kaminska, P. Eng.
Supervisor
Professor _____

Dr. Andrew Rawicz, P. Eng.
Internal Examiner
Professor
School of Engineering Science _____

Dr. Wei-Chih Wang
External Examiner
Research Associate Professor
Department of Mechanical Engineering
University of Washington _____

Date Defended/Approved: November 3, 2015

Abstract

This thesis presents the development of a technology employing printed circuit board (PCB) technology to facilitate the performance and translation of point-of-care (POC) biosensing and bioprocessing devices toward practical products. Key features of the proposed technology are a universal, standardized platform and a set of techniques, featuring integrated functional units, three-dimensional (3D) configurations, convenient device-instrumentation interconnections, and industry-compatible precision manufacturing. The developed technology aims to incorporate and fabricate multiple functional units into a POC device with a compact configuration to perform bio/chemical sensing or processing that requires complex experimental conditions.

In this thesis, PCB technology is employed to facilitate the development of three example biosensing and bioprocessing applications for proof of concept. First, the capability of using PCB substrates for complex assembly of functional components is demonstrated to facilitate the development of a chemistry-based enzyme assay. Proof-of-concept glucose-6-phosphate dehydrogenase (G6PD) deficiency assays are developed with integrated pH sensing units and temperature control units on boards. The assay is found to determine the G6PD level of a sample within 2 minutes.

PCB technology is demonstrated to not only form an integrated platform but is also utilized in the fabrication of functional elements for biosensing and bioprocessing devices and systems. The second demonstrator is a molecule-based quantitative polymerase chain reaction (qPCR) device. A method is employed in this work to produce arrays of electrochemical biosensors and thermal cyclers using a three-metal PCB technology. The electrochemical performance and surface morphology of the biosensor microelectrodes are characterized and evaluated. The qPCR experiments are performed with 95% PCR efficiency and the detection limit of 59 deoxyribonucleic acid (DNA) copies.

The third demonstrator is a cell-based on-board cooling rate controlled cryopreservation device. The possibility of meso-scale integration between the platform, sample storage and instrumentation is demonstrated in this work to facilitate the development of bioprocessing applications. On-board cooling-rate-controlled cryopreservation devices for use in low-temperature (-80°C) environments are developed with disposable, biocompatible polydimethylsiloxane (PDMS) storage chambers on top of localized feedback-controlled heaters on boards. These devices were able to maintain a stable cooling rate as low as 1°C per minute.

Based on the work presented in this thesis, the future development plan and possible business models for the proposed technology are envisioned from academic and industrial perspectives to realize POC biosensing and bioprocessing applications toward commercialization.

Keywords: Point-of-Care; Biosensing, Bioprocessing; Biomedical Micro-electro-mechanical Systems; Printed Circuit Board

Dedication

To my mother and sister.

Acknowledgements

I acknowledge the National Science and Engineering Research Council of Canada, the Canada Foundation for Innovation and CMC Microsystems for funding and/or providing software tools, fabrication equipment, and testing equipment, which made this research possible. This work made use of 4D LABS and School of Engineering Science shared facilities in the Simon Fraser University. I would also like to especially thank Enigma Interconnect Corp. and its president, Mr. Mark Pillon, for industrial support and for the in-kind donation of materials for the printed circuit boards and Mr. Shih-Shun Lan, Victor Adamik, John Parsons, Bill Yip at the Enigma Interconnect Corporation for advice and assistance in fabrication.

I also acknowledge Mrs. Jenny Lum for her expertise and great assistance in biochemical techniques and facilities; Mr. Graham Hallson for his training and assistance in biochemical experiments; Mr. Scott Malfesi for his help with instrumentation; Dr. Rosemary Smith from the University of Maine, Orono, for providing ISFETs; Mr. Jing-Kai Lin for technical discussion about the project of enzyme assays; Yasong Li (and her supervisor Carlo Menon) for assistance with the standard AFM techniques; Graeme Suppes for the equipment setup of the cyclic voltammeter; and Environmental Bio Detection Products (EBPI) Inc. for the inspiration of the qPCR project.

I would like to offer my great appreciation to my senior supervisor, Dr. Bonnie Gray, for her huge support; to my supervisor, Dr. Bozena Kaminska, for her significant suggestion; Dr. Andrew Rawicz for his help and spirits; Dr. Wei-Chih Wang for his efforts in this examination; and finally my co-workers, friends and family for all professional or mental support.

Table of Contents

List of Tables

List of Figures

List of Acronyms

3D	Three Dimensional
AFM	Atomic Force Microscope
CFU	Colony-Forming Unit
Ct	Threshold Cycle Number
FPGA	Field-Programmable Gate Array
DNA	Deoxyribonucleic acid
FR-4	Fiberglass epoxy resin
G6PD	Glucose-6-Phosphate Dehydrogenase
ISFET	Ion-Selective Field-Effect Transistor
LPISM	Liquid Photo-Imaging Solder Mask
MB	Methylene Blue
MEMS	Micro Electro Mechanical System
NADP	Nicotinamide Adenine Dinucleotide Phosphate
NADPH	Nicotinamide Adenine Dinucleotide Phosphate in Reduced Form
OBM	Original-Brand-Manufacturer
ODM	Original Design Manufacturer
OEM	Original Equipment Manufacturer
PCB	Printed Circuit Board
PDMS	Polydimethylsiloxane
PID	Proportional, Integrated, Differential
PMMA	Polymethyl Methacrylate
POC	Point-of-Care
qPCR	quantitative Polymerase Chain Reaction
SEM	Scanning Electron Microscope

Chapter 1.

Introduction

1.1. Biomedical Micro-electro-mechanical Systems

Micro electro mechanical systems (MEMS) techniques have been widely used by academic researchers to develop promising biosensing and bioprocessing applications on miniaturized silicon/glass chips of millimeters or centimeters in size [1-5]. With the advantage of small size, these devices are expected to be utilized near and right after sampling events, resulting in point-of-care (POC) diagnostics, while also proving to be cost-effective, accurate, rapid, and simple to operate [6]. Despite the fact that MEMS techniques are suitable for the fabrication of sensing/actuating elements at the micro-scale and for planar devices, they are not designed to configure devices in the slightly larger meso-scale or those with 3-dimensional (3D) geometries.

Desired configurations of POC devices are expected to incorporate multiple functional units to perform biosensing or bioprocessing tasks with complex experimental condition requirements in a compact and portable format. These functional units can be sensors (e.g. micro-electrodes, ion-selective field effect transistors, thermometers), other components (e.g. heaters, electrodes, coils), or fluid handling elements (e.g. sample loading and chambers). Academic researchers commonly find it challenging to realize a device which is expected to execute a task requiring, for example, temperature control and the detection of a certain analyte at the same time. In order to fulfill all experimental conditions for a complex analysis, this challenge encountered by academic researchers further results in that most attempts to build a lab on a chip often more resembles a chip in a lab [7] instead.

Additionally, interfaces between functional units, samples, and instrumentation involve electrical and mechanical interconnections, so that, for instance, an electrical signal from microelectrodes in a device can be read by an external electronics through soldered connections. An integrated configuration requires not only a compact assembly of components on a platform but also interconnections between the device and instrumentation. Components such as sensors and actuators usually require several circuit traces and pins to connect to external electronics that analyze or control these components by receiving or transmitting signals; however, traditional MEMS fabrication of POC devices does not render adequate flexibility for system integration due to the constrained material properties and manipulation of glass/silicon substrates.

As presented in an article written by Holger Becker (CSO of microfluidic ChipShop in Germany) [8], reliable and cost-effective manufacturing is one of the most crucial success factors for commercializing a POC device or system. However, most clean-room and fabrication facilities in academic organizations lack industry-grade machining tools such as injection molding/printing, hot embossing, and parts assembly, as these manufacturing approaches are only suitable for the mass production of optimized and finalized products. On the other hand, academic researchers require reconfigurable and customized processes, such as MEMS techniques, at research and development phases.

In order to overcome these challenges and facilitate the translation of POC biosensing and bioprocessing devices toward practical usage and commercialization, new design platforms and manufacturing processes are required. Such design platforms and manufacturing processes as problem-solving tools should have the following desired characteristics:

- Adoption of Industry-compatible and standardized materials and methods
- Integration of multiple functional units to achieve complex experimental conditions
- Reliable and convenient interconnections between devices and instrumentation
- Miniaturized format for portable purposes

- Competitive performance of target biosensing and bioprocessing applications

- Possibility of being integrated with microfluidic platforms

1.2. Printed Circuit Board Technology

Addressing integration and interconnection problems, a universal, standardized platform and a set of techniques are urgently required by researchers to customize their devices with integrated functional units, industry-compatible precision manufacturing, and convenient system interfaces to perform complex biosensing or bioprocessing tasks in parallel. The main objective of this thesis is to utilize printed circuit board (PCB) technology as a new option and problem-solving tool for academic researchers to facilitate the development and translation of their biosensing or bioprocessing devices into practical products. The proposed technology is composed of a variety of highly scalable and automatic industrialized processes that specialize in precisely manufacturing integrated platforms for multifunctional components to form compact configurations with resolutions down to the micro-scale. The integrated platforms aim to improve the integration problems of current bio-MEMS technologies. The proposed processes aim to build compact configurations that multiple functional units, such as bio/chemical sensors, temperature control elements, and fluid handling elements, are either directly fabricated or packaged on boards to conveniently connect with instrumentation.

The manufacturing processes of PCB technology for biosensing and bioprocessing applications are introduced in this section. As shown in Figure 1.1, these processes consist of (1) computer aid design (2) computer aid machining (e.g. drilling, milling), (3) electroless plating metals, (4) dry film photolithography, (5) chemical etching, and other processes (e.g. solder mask protection, multilayer lamination) [13].

First, layer-by-layer schematics are drawn using an electronic design automation software tool (e.g. EAGLE, OrCAD) with a finest resolution limit of around 50 μm. The layout should indicate placements and dimensions of components, such as sensors, and electrical interconnections, such as circuit lines, pin holes, and contact pads. Different patterns of metals can also be plotted at different design layers in the software. After the

design process, the Gerber files are generated. Meanwhile, the material types and the thickness of their substrate and deposited metals should be specified.

Second, the Gerber files are converted into a series of processes. A bared board usually made of fiberglass epoxy resin (FR-4) or polyimide is first machined by a computer-aid-manufacturing tool where all pin holes on the board are precisely drilled with small-diameter drill bits made of solid coated tungsten carbide.

The board is then cleaned by a process called micro-etch consisting of the immersions of the board into monopersulfate and peroxide based chemicals to remove unwanted surface smears and contaminations. To create conductive layers on the surface of the board, thin-film (at thinnest 1 μm) copper is deposited by electroless plating. The electroless plating process enables a wider range of film thickness and is simpler than sputtering; it is achieved by the process of reactions between a reducing agent with metal ions on the metallic substrate and non-conductive substrates after surface pre-treatment and activation.

A dry film resist is then laminated on the board by hot pressing and rolling, followed by photolithography, which consists of selective UV exposure through a photomask and chemical development patterns on a photomask can be optically printed by a laser photoplotter or directly projected on the dry film using a digital maskless photoimager (minimum feature size = 50 μm, accuracy = 3 μm). The photo-patterned dry film resist acts as a protective layer for the area of copper film being kept during etching.

The copper film is spray etched by ammonium persulfate. In spray etching, the etchant solution is distributed over the board's surfaces by nozzles with controlled flow rate, temperature, and etchant composition ensuring predictable and efficient etching rates. Note that the thin-film copper can also be patterned in an additive way (without etching), and in this way the electroless plating is executed after photo-patterning the dry film resist so that only the uncovered area undergoes copper deposition.

After the dry film resist is stripped, the patterned thin-film copper acts as a seeding layer where multiple layers of different metals, such as silver, nickel, gold, and tin, can be

formed by electroless plating on top through processes involving several immersions into chemical baths in an automatic production line.

Multilayer boards are available by hot pressing several boards together where layers connect with each other through vias, which are the conductive drilled holes. Solder masks (thickness = 50 μm) can be screen-printed and cured to protect metallic layouts on the board while to leave soldering sites for electrical connections between the board and instrumentations. Finally, multiple components such as temperature sensors, pH sensors, and microfluidic chambers can be placed and attached onto the boards.

Depending on the manufacturers, various types of equipment and chemicals are used for similar purposes. Common suppliers for the chemicals are DuPont, Dow, Eternal, and Taiyo, specializing in dry film resists, board cleaning, metal plating, solder masks and etc. Other suppliers for materials, such as Ventec and Kodak, manufacture FR-4 laminates and silver films respectively. Details are not mentioned here, such as that there are also many other companies specializing in equipment and tooling for computer-aid machining, photo-plotter, mask-less photo-imager, chemical baths, spray etching, hot pressing, electrical testing, X-ray inspection, silk screen printer, and so forth [14].

Many other researchers have envisioned using PCB for biosensing and bioprocessing applications such as cell lysis and nucleic acid extraction [9-12]; however, this prior research primarily focuses on using the board solely as the substrate of the devices instead of using PCB technology to manufacture the biosensing or bioprocessing elements. In addition, to our knowledge no prior research addresses the challenge of complex experimental condition requirements (e.g. temperature control and electrochemical detection of an analyte at the same time), despite the fact that complex experimental conditions are usually required by various biosensing and bioprocessing research.

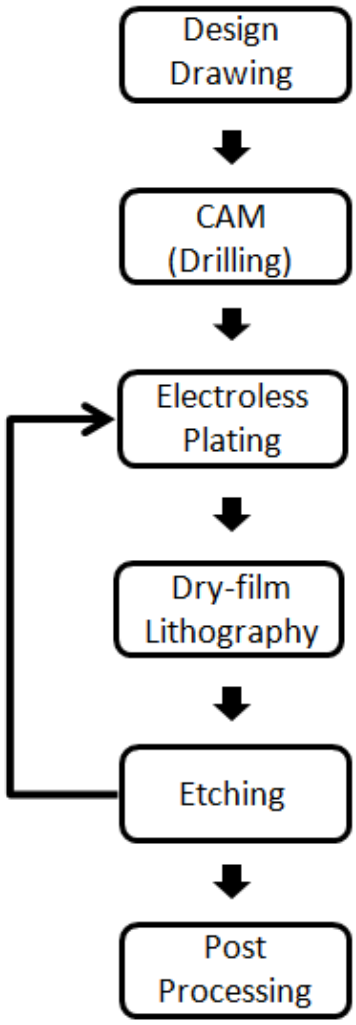

Figure 1.1. An example process flow of the manufacturing techniques

1.3. Our Solution

Figure 1.2 illustrates the overall concept of the technology presented in this thesis that is used to develop three important demonstrator devices that each make significant contributions to their respective areas, and reply on aspects of the technology shown in Figure 1.1. The technology is shown integrated together with an example microfluidics chamber made of polymers. The biosensors and bioprocessing devices (e.g. ion-selective field effect transistor, microelectrodes, temperature sensors, and heater) are all integrated on the PCB; either directly fabricated using multiple different metals as needed, or as components attached to the PCB. These components and microfluidic chambers/channels are placed on the top and bottom sides of the PCB to form a 3-dimensional (3D) configuration with electrical interconnections.

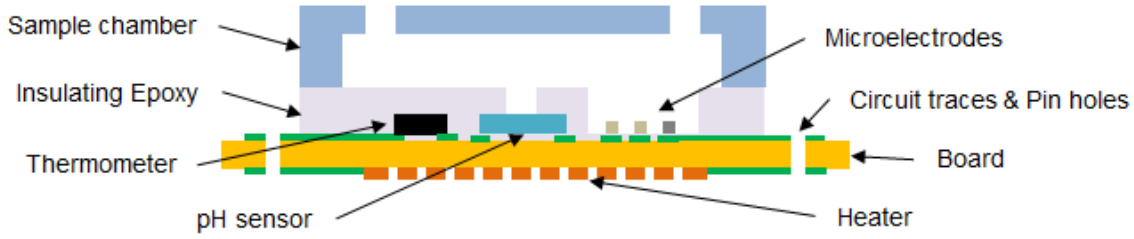

Figure 1.2. Overall concept of the technology: Multiple functional units (e.g. microelectrodes, heater, thermometer, pH sensor) are fabricated or incorporated on a board using PCB technology to implement biosensing or bioprocessing tasks in a sample chamber made of polymers. Circuit traces and pin holes allow these components to be connected to external instrumentation. Note that Electrodes can be fabricated in multiple different metals by electroless plating.

This thesis describes the use of this PCB-based technology in the development of POC biosensing and bioprocessing to develop such a platform. The characteristics of this technology are:

- Industry-compatible standardized design and manufacturing processes
- Integration/Fabrication of multiple functional units to achieve complex experimental conditions

- Reliable and convenient interconnections between devices and instrumentation
- Miniaturized format for portable purposes
- Competitive performance of target biosensing and bioprocessing applications
- Possibility of being integrated with microfluidic platforms

To attain these characteristics, the thesis has the following key technological objectives:

1. Develop manufacturing processes for POC biosensing and bioprocessing applications based on the industrialized materials and methods of PCB technology to ensure the feasibility of future mass production.
2. Utilize the multilayer feature of PCB technology to fabricate or incorporate multiple functional elements for POC biosensing and bioprocessing in 3D configurations.
3. Establish reliable and convenient solder-able surface-mount or pin-hole interconnections between on-board devices and external instrumentation.
4. Achieve manufacturing resolutions down to the micro-scale to ensure the compactness of devices.
5. Demonstrate and compare the performance of the target POC biosensing and bioprocessing applications with bench-top standards.
6. Propose a future plan for on-board microfluidics integration.

To achieve these objectives, combinations of PCB technology (specification shown in Table 1.1) and clean-room microfabrication can be arranged to achieve various design requirements at component, configuration, and system levels for developing biosensing and bioprocessing devices. For example, microelectrodes made of gold and silver along with heaters can be fabricated using PCB techniques for electrochemical sensing with temperature control; other microfabricated components, such as transistors,

temperature sensors and microfluidic structures, can be surface mounted or attached on PCB platforms. All functional units are properly placed and connected to instrumentation enabling compact configurations and user-friendly system interfaces. The industry-compatible and standardized but reconfigurable design and manufacturing processes of PCB technology also ensure future mass production of the devices.

Table 1.1. Specification of the Manufacturing Processes

Minimum Feature Size	50 µm
Accuracy	3 µm
Minimum Board Thickness	130 µm
Minimum Metal Thickness	1 µm
Minimum Soldermask Thickness	50 µm
Minimum Drilling Diameter	200 µm

Two major novelties of the proposed solution over other PCB-based platforms [9-12] are (1) integration of multiple functional units in 3D configurations and (2) direct fabrication of biosensing and bioprocessing elements. Many biosensing and bioprocessing applications requires the integration and direct fabrication of multiple functional units in 3D configuration to allow complex experimental conditions to be achieved in parallel. For example, pH-based enzyme assays require the measurement of pH value under certain temperature; quantitative polymerase chain reaction (qPCR) experiments require the measurement of electrochemical signals under thermal cycling. Without the novel characteristics, the development of POC devices for these two applications would be challenging. In this thesis, the novel characteristics of the proposed technology not only facilitate the translation of biosensing and bioprocessing devices into practical products, but also are keys in the realization of novel demonstrator devices that themselves push the boundaries of research in their respective areas.

1.4. Proof-of-Concept Demonstrations

In the following three chapters, the three novel proof-of-concept examples of using PCB processes and platforms to facilitate the development of biosensing and bioprocessing applications are presented that rely on various aspects of the proposed technology for realization. These three example applications were each selected as they represent key applications in chemistry-, molecule- and cell-based research that each benefit from the technology developed for this thesis. Not only do the demonstrators showcase various key aspects of the developed technology, they each push the envelope of research in their respective domains.

First, the capability of using PCB substrates for complex assembly of functional components is demonstrated to facilitate the development of a chemistry-based enzyme assay. The use of PCB technology in this work ensured the integration of multiple components into a POC device and the interconnection between the device and instrumentation. In this work, multiple functional units, which include a pH sensitive ion selective field effect transistor, a reference electrode, a temperature sensor and a heater, were incorporated in a 3D on-board configuration. Arrays of contact pads and pin holes were established to ensure reliable interconnections between these components and external instrumentation. Utilizing the proposed technology, a pH based detection method was for the first time developed to demonstrate the outstanding result that glucose-6-phosphate dehydrogenase (G6PD) deficient samples could be determined within 2 minutes.

Second, the capability of directly using PCB techniques in fabricating biochemical sensors and components and forming an array of 3D configurations is demonstrated to facilitate the development of molecule-based quantitative polymerase chain reaction (qPCR) experiments. In this work, a three-metal printed-circuit-board process was for the first time employed to produce arrays of electrochemical microelectrodes and thermal cyclers. This work demonstrated that complex experimental requirements could be achieved simultaneously to realize the detection of a certain analyte. In this work, the electrochemical performance and surface morphology of the biosensor microelectrodes were characterized and evaluated. The quantitative polymerase chain reactions were

performed with 95% PCR efficiency and a detection limit of 59 Deoxyribonucleic acid (DNA) copies.

Third, the possibility of using PCB to facilitate meso-scale sample storage and integration of cell-based on-board cooling rate controlled cryopreservation was investigated. On-board cooling-rate-controlled cryopreservation under low-temperature environments (-80 °C) is for the first time developed with disposable, biocompatible polydimethylsiloxane (PDMS) storage chambers on top of localized feedback-controlled heaters on boards. The devices were able to maintain a stable cooling as low as 1 °C per minute. In this work, the use of PCB technology ensures user-friendly and convenient interfaces between the platform, sample, and instrumentation to form a bioprocessing system.

These three prototyped devices also showcase various aspects of the developed technology, specifically: (1) a standardized, scalable, but customized manufacturing processes ensuring future mass production, (2) the integration/fabrication of multiple functional units to achieve complex experimental conditions, (3) reliable and convenient interconnections between devices and instrumentation, (4) a miniaturized format for portable purposes, and (5) comparable performances to bench-top approaches.

Chapter 2.

Development of Rapid Screening for Glucose-6-phosphate Dehydrogenase Deficiency Prior to Malaria Treatment Utilizing On-board pH-based Electrochemical Assay

This chapter presents a prototyped assay to detect glucose-6-phosphate dehydrogenase (G6PD) deficiency before administration of an anti-malaria drug, which may cause potentially lethal acute hemolytic anemia in patients with G6PD deficiency. The proton production from a chemical reaction catalyzed by G6PD was for the first time measured to reflect the G6PD activity in a blood sample. The device consists of a pH sensor, a temperature control unit, and a fluidic sample well, which were all integrated on a print circuit board (PCB). The experimental results indicate that samples with G6PD deficiency can be diagnosed within two minutes rendering a point-of-care assay for rapid screening. This work has been published in the Journal of the International Measurement Confederation.[1]

In this work, the prototyped device was made by automatic industrial manufacturing processes, showcasing industry-compatible standardized design and manufacturing processes. Multiple components (i.e. pH sensor, thermometer, and heater) were incorporated for temperature control and pH measurement, showcasing the integration of multiple functional units to achieve complex experimental conditions. All these components were connected to external instrumentation through contact pads and solderable pin holes, showcasing reliable and convenient interconnections between devices and instrumentation. The miniaturized format of the prototyped device ensures its portability for POC diagnostics. The experimental results indicate the competitive performance of the proposed G6PD deficiency rapid screening to prior arts.

[1] Tseng HY, Malfesi S, Lum J, Gray BL. Development of rapid screening for glucose-6-phosphate dehydrogenase deficiency prior to malaria treatment utilizing on-board pH-based electrochemical assay. *Measurement 2015;* 73:158-61.

2.1. Introduction

Glucose-6-phosphate dehydrogenase (G6PD) is an enzyme that protects erythrocytes from oxidative injury. An estimated 400 million people worldwide are affected by G6PD deficiency [15], a genetic enzyme disorder leading to fatal hemolysis of erythrocytes under exposure to certain medications [16]. The drugs comprising the 8-aminoquinolone group (e.g. primaquine, dapsone, and tafenoquine), are anti-malaria drugs commonly used to cure Plasmodium vivax hypnozoites and Plasmodium falciparum gametocytes; however, these drugs can cause acute hemolysis in individuals with G6PD deficiency [17]. With the higher prevalence of G6PD deficiency in regions endemic to malaria [18], rapid assessment of the G6PD statuses of patients prior to administering anti-malaria drugs is therefore desirable to minimize the risk of adverse reactions for patients simultaneously possessing G6PD deficiency.

G6PD is a cytosolic enzyme that catalyzes the following chemical reaction:

$$\text{D-glucose 6-phosphate} + NADP^+ \leftrightarrow \text{6-phospho-D-glucono-1,5-lactone} + NADPH + H^+$$

In this enzymatic reaction, G6PD reduces nicotinamide adenine dinucleotide phosphate (NADP) to its reduced form (NADPH) while oxidizing glucose-6-phosphate (G6P) and producing a proton [19]. To quantitatively characterize the level of G6PD activity, a conventional test utilizes a UV (340 nm) spectrophotometer to measure NADPH production in the reaction. This test is a standardized protocol in centralized laboratories and provides accurate results; however, the complicated and costly optical setup of the spectrophotometer constrains its capability for point of care diagnosis [20].

Few qualitative chromatographic G6PD tests (e.g. BinaxNOW G6PD test™ and CareStart™) have recently been developed to respond to the need of rapid screening of G6PD deficiency [21,22]. These test devices consist of a flow test strip containing a nitro blue tetrazolium dye to be reduced into its concomitant blue formazan product in a G6PD enzymatic reaction. The resulting color change is read visually at the test read time to indicate whether or not the sample is presumed to be deficient in G6PD enzyme activity. However, the chromatographic test relies solely on the user's subjective judgement of color change. Furthermore, the correct performance of the BinaxNOW G6PD test™ can

only be guaranteed in the temperature range of 18-25 °C, rendering it potentially impractical for use in tropical regions.

In this chapter, a prototype pH-based G6PD assay is proposed to measure the production of protons (H+) and resulting pH change in the G6PD enzymatic reaction using an integrated set of a pH sensing unit, a temperature control unit and a testing well on a printed circuit board (PCB). Ion-selective field-effect transistors (ISFETs) have been studied since the 1970's as an alternative to conventional glass electrodes for pH measurement with the advantages of better resistance to breaking, easier maintenance for use in biological applications, and more stable, accurate reading over a wide temperature range [23]. Despite the fact that ISFETs have been widely developed to detect numerous analytes such as glucose, penicillin, urea, creatinine, etc., by immobilizing enzyme layers at the gate [24], there is no yet commercial-available product specialized in rapid screening for G6PD deficiency employing pH based detection. The goal of this work aims to determine the G6PD deficiency for the first time by directly measuring the pH change as a result of proton production from the G6PD enzymatic reaction. The integrated design on the PCB platform ensures convenient electrical interconnections to external instrumentation and standardized manufacturing with potential toward mass production. Compared with the chromatographic methods, the pH-based method allows not only qualitative but also the quantitative determination of G6PD levels. Compared with the conventional spectrophotometric method, our proposed system provides better portability and enables point-of-care diagnostics. In this chapter, a proof-of-concept work promising the novel detection mechanism and an integrated sensing platform is presented.

2.2. Material and Methods

The design consists of an ISFET (length: 2 mm, width: 1.5 mm, height: 0.5 mm), a reference electrode (length: 3 mm, diameter: 0.5 mm), a temperature sensor (length: 1.5 mm, width: 1 mm, height: 0.5 mm), and a heater (length: 7 mm, width: 5 mm) on a customized printed circuit board (PCB). The ISFET and the reference electrode were designed to measure the pH change derived from the chemical reaction catalyzed by G6PD. The temperature sensor and the heater were used to maintain a constant temperature during the measurement, eliminating possible influences of temperature on the pH sensor and the enzyme activity. The overall layout of the device before encapsulation and fluid sample well attachment is shown in Figure 2.1. The PCB was designed using commercial software (EAGLE 6.4.0), and manufactured in an industrial facility (Enigma Interconnect Corp., Burnaby, BC). A total of 12 contact pads and corresponding pin holes (three for the ISFET, one for the reference electrode, six for the temperature sensor, and two for the heater) were made for electrical interconnections between the components and instrumentation. The n-channel ISFET was fabricated using standard IC technology in the microfabrication clean-room facility [25,26]. The ISFET was obliquely placed and wire bonded on the board. A subsequent epoxy encapsulation left only the gate area uncovered. An Ag/AgCl wire reference electrode was also obliquely placed and bonded by a conductive epoxy on the board. A serpentine-shaped copper wire was electrolessly plated and photo-patterned on the back of the board to form a heater. A digital temperature sensor (TMP112, Texas Instruments) was soldered on the board. Insulating epoxy was then carefully casted and cured to protect these components. Finally, a biocompatible polydimethylsiloxane (PDMS) well was attached on top of the sensing area to hold a liquid sample for testing. The temperature of the device was maintained closed-loop at 37 °C by the temperature sensor and the heater, where the power input was regulated by a proportional, integrated, differential (PID) feedback control in a microcontroller (Arduino). During pH measurements, the current (IDS) through the ISFET was measured and converted by an electrometer circuit to a voltage signal reflecting the pH value of the tested solution. The ISFETs were calibrated using standardized pH buffers at pH 4, 7, and 10 (VWR).

Different levels of G6PD activities were screened by the pH based assay measuring the pH change due to the proton production from the enzymatic reaction. The experiments were performed using G6PD samples in stabilised human red cell hemolysate manufactured by the Trinity Biotech at three control levels: deficient level (G5888), intermediate level (G5029), and normal level (G6888). Two more G6PD levels to be tested were prepared with 1-fold dilution of the samples at the normal and intermediate levels to more accurately observe the performance of G6PD detection. The enzyme concentrations of the deficient, intermediate, and normal levels were first characterized by monitoring the absorbance of NADPH in tested solutions at 340 nm (A340) with a UV spectrophotometer (Genesys 10, Thermo Scientific) and a commercialized G-6-PDH kit (Trinity Biotech) at 25 °C. For the pH based assay, the master mix was prepared to contain 1 mM NADP (N5755, Sigma Aldrich), 2 mM G6P (G7879, Sigma Aldrich), 10 mM $MgCl_2$ (VWR), and phosphate buffer (18 nM NaH_2PO_4 and 28 nM Na_2HPO_4) (VWR). Note that the oxidation of G6P by G6PD is specific; the G6P substrate was saturated in our tests to minimize unwanted proton production which might occur through other enzymes such as 6-phosphogluconate dehydrogenase. The pH of the master mix and samples were adjusted to be 7.8 by NaOH and HCl titration. Note that a pH drop, instead of an absolute pH value, was derived in this work, therefore influences of a minor variation from the desired initial pH level may be minimized. A plastic body pH electrode (S350CD, Sensorex) was used to assist in pH calibration and some measurements. In each experiment, 47 µL of the master mix was first injected into the well and maintained at 37 °C. Next, 3 µL of the G6PD sample was injected into the master mix and thoroughly stirred by a pipette for 3 seconds. The 3-second stirring was the minimal time required to ensure enough mixing of the solution and set to standardize the process for all experiments. The enzymatic reactions may be limited without the stirring, whereas the data recording may be delayed with extra stirring. The transient pH change of the tested solution was monitored at 5 seconds sampling intervals over a 2-minute period. In order to understand how the expected pH drop of the sample solution affected the enzyme activity, the UV spectrophotometer was employed to monitor the absorbance of NADPH at 340 nm (A340) in a tested solution. In each experiment, 3 mL of the tested solution was made containing 2.85 mL of the master mix and 150 µL of the G6PD sample (1.5 U/mL) (G6378, Sigma Aldrich).

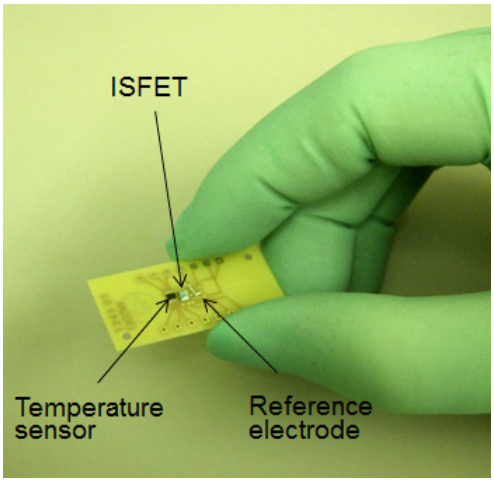

(a)

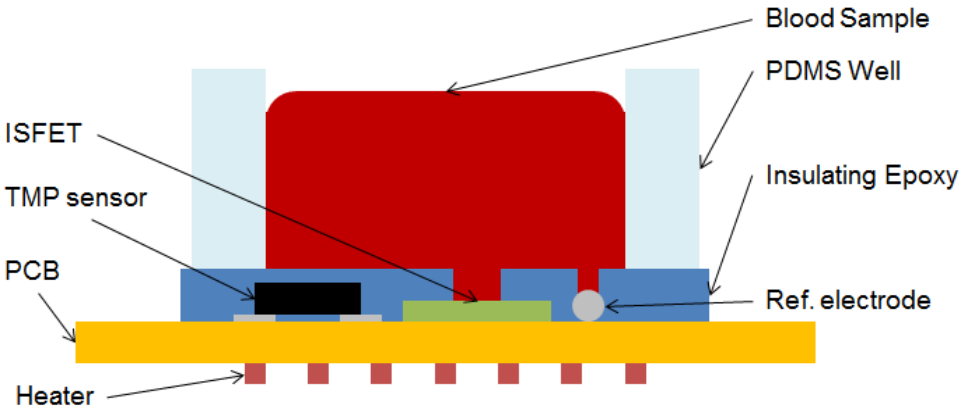

(b)

Figure 2.1. (a) The integrated device with a temperature sensor, ISFET, and reference electrode on a printed circuit board and a heater on the back. (b) Cross-sectional diagram of the overall design of the device from the front view (the figure is not to scale).

2.3. Results and Discussion

Samples of three G6PD levels, deficiency, intermediate and normal, were characterized by the conventional spectrophotometric method using the commercialized kit and a standardized protocol according to the product information. The slopes of the linear curves were derived, calculated and followed by a temperature correction that were given by the Trinity Biotech, indicating that the enzyme concentrations of the three G6PD levels were respectively 0.070, 0.40, 1.27 U/mL at 37 °C (n = 3, S.D. = 0.028, 0.081, 0.37 respectively). These values of concentration were set to be golden standards.

The pH values of the tested solutions containing samples with different G6PD levels were measured in this work. The pH change (Δ pH) was derived by finding the difference between the current pH reading and the initial pH reading, which was around pH 7.8. As shown in Figure 2.2a, the Δ pH for five G6PD levels was recorded in terms of time. The pH dropped the most dramatically for the sample with normal G6PD level; the next largest changes occurred for samples with the 0.5×normal, intermediate, 0.5×intermediate, and deficient levels, respectively. These results indicate that the tested solution became much more acidic when more G6PD was present in the sample solution. This agrees with the theory whereby more proton production from the enzymatic reaction should lead to lower pH in the solution.

To analyze the pH curves for different G6PD levels, a threshold, Δ pH = 0.5, was assigned. The time required for the pH change to reach the threshold was used to reflect the enzyme concentration or activity in the solution. In Figure 2.2b, the time required to meet the threshold pH change in terms of the G6PD level is shown. A non-linear relationship is observed with a 2nd order polynomial trend. This may be explained that two different mechanisms contributed to the non-linear trend: less proton production and decreased probability of proton detection by the sensor in the samples with lower enzyme concentrations. The results in Figure 2.2a and b provide quantitative information about the pH based assay for its future use in G6PD detection.

The blood samples used in the experiments were based on 12 g/dL hemoglobin. For this assay, the cut-off G6PD deficiency was set at 4 U/g hemoglobin [21] which is equivalent to 0.48 U/mL for the samples used in this work. According to the results

presented, the time required for the pH change to reach the threshold for the cut-off G6PD deficiency is approximately 40 seconds. These results suggest that samples requiring more than 40 seconds reaching the threshold pH change should be considered as G6PD deficiency. In our results, a maximal ± 17% of error was observed at one standard deviation. The test can be completed in two minutes, indicating that the device may serve as a rapid screening for G6PD deficiency.

It may be postulated that the acid environment may inhibit the enzymatic reaction; therefore, in order to understand if the pH drop affects the efficiency of the enzyme, a standardized A340 test was performed for each sample. It was founded that the NADPH product increased linearly (R^2 = 0.9984) during the testing period (5 min), indicating that the pH drop did not affect the efficiency of the enzymatic reaction in the range of the testing period for the pH experiments. Effects of testing temperature on either the pH sensor or the enzymatic reaction were also tested; however, no variation was observed from the experimental results in the range of 25-37 °C, possibly due to the minor change of enzyme activities compared with the detection error. Based on the preliminary results, the temperature range of 25-37 °C worked for our experiments; nevertheless, it is suggested that more tests should be executed; otherwise, a constant temperature (e.g. 37 °C in this work) should be maintained using the on-board temperature control system for all tests.

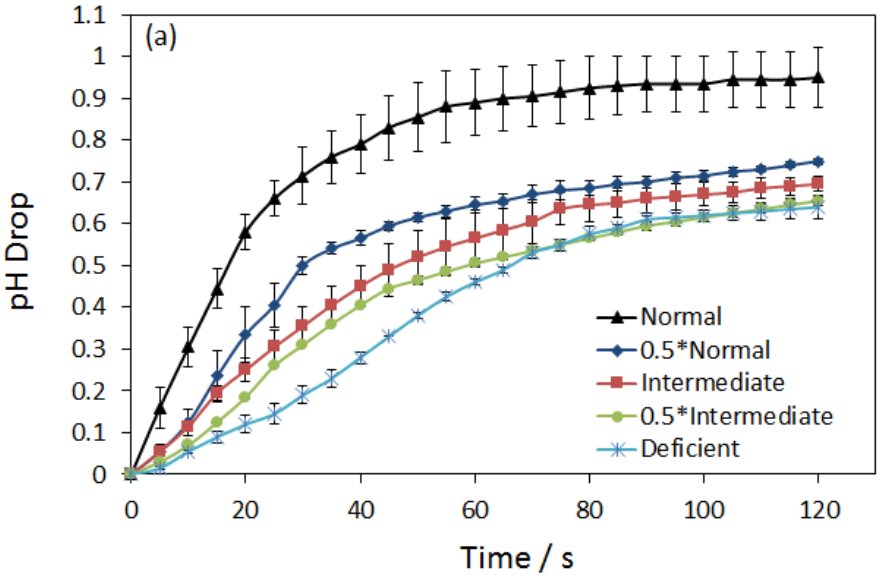

(a)

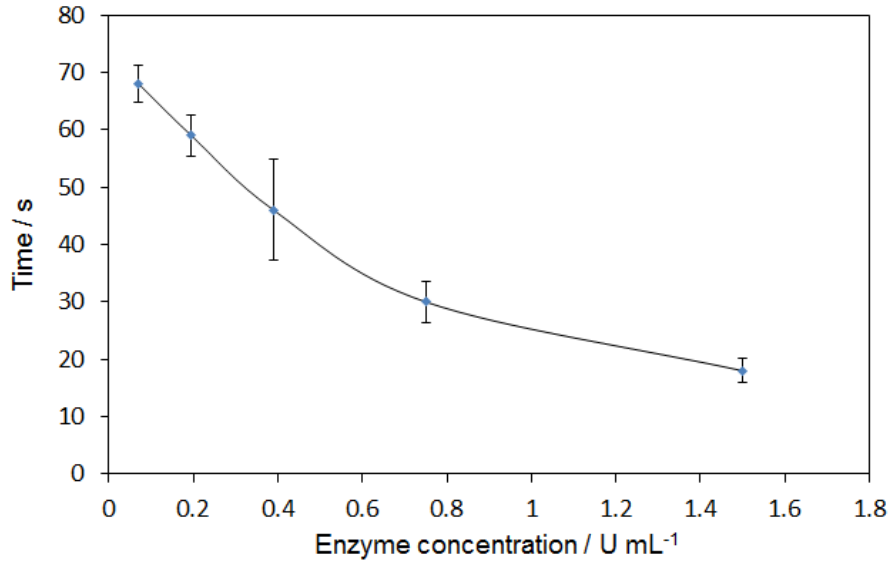

(b)

Figure 2.2. (a) The pH drop of the five different G6PD levels monitored over a 2-minute time period. (b) The required time for the different G6PD levels to reach the threshold pH drop (all error bars shown on one standard deviation).

2.4. Conclusion of the Work Presented in this Chapter

A proof-of-concept G6PD deficiency detection assay was developed that employs the principle of measuring the proton production from the above-mentioned chemical reaction catalyzed by G6PD. To demonstrate the device toward a point-of-care assay, sensors and temperature control units were integrated on a printed circuit board. The quantitative information of the G6PD assay was characterized and found to determine the G6PD level of a sample within 2 minutes. The results indicate the possibility of the method for future implementation in point-of-care diagnosis which would provide a new and effective tool in anti-malarial therapy. In order to achieve a more user-friendly process of sample loading, microfluidic liquid control including reagent guiding and mixing, should be designed and realized in future prototypes. Process optimization and formal clinical testing with a wide range of blood samples and interferences should also be performed before commercialization. It is believe that, based on the advantages of fast diagnosis, reusability, temperature insensitivity, and portability; the pH-based electrochemical assay will support the rapid screening for G6PD deficiency prior to malaria treatment.

In this work, the prototyped device was made by automatic industrial manufacturing processes, showcasing industry-compatible standardized design and manufacturing processes. Multiple components (i.e. pH sensor, thermometer, and heater) were incorporated for temperature control and pH measurement, showcasing the integration of multiple functional units to achieve complex experimental conditions. All these components were connected to external instrumentation through contact pads and solderable pin holes, showcasing reliable and convenient interconnections between devices and instrumentation. The miniaturized format of the prototyped device ensures its portability for POC diagnostics. The experimental results indicate the competitive performance of the proposed G6PD deficiency rapid screening to prior arts.

Chapter 3.

Development of an Electrochemical Biosensor Array for Quantitative Polymerase Chain Reaction Utilizing Three-metal Printed Circuit Board Technology

A compact biosensing system is presented that contains an array of devices composed of three-microelectrode electrochemical sensors and resistive heaters. The devices are intended for employment in quantitative polymerase chain reactions (qPCR) in multiple chambers that can be controlled via microcontroller. Arrays of sensors and heaters were developed using an inexpensive advanced printed circuit board (PCB) technology featuring three different metals. The three-microelectrode sensors were fabricated by a new series of photolithographic and electroless plating processes. The surface morphology of the microelectrodes was characterized by several imaging techniques, including scanning electron microscopy and atomic force microscopy. The electrochemical properties of the microelectrodes were studied by cyclic voltammetry in order to estimate the active electrochemical surface area by solving the Randles-Sevcik equation. The on-board thermal cyclers were realized by feedback control embedded in a portable microcontroller. qPCR with methylene blue as the redox indicator were carried out as an example of biosensing with the proposed devices, and the results indicate that the prototype array is able to serve as an inexpensive, practical platform for mass production of portable point-of-care instrumentation containing arrays of addressable heaters and sensors. This work has been published in the journal, Sensors and Actuators B: Chemical[2].

In this work, the biosensor array was made by automatic industrial manufacturing processes, showcasing industry-compatible standardized design and manufacturing processes. Biosensing elements (i.e. microelectrodes and heater) were fabricated for electrochemical measurement and thermal cycling, showcasing the integration of multiple functional units to achieve complex experimental conditions. All these components were

[2] Tseng HY, Adamik V, Parsons J, Lan S, Malfesi S, Lum J, Shannon L, Gray B, Development of an electrochemical biosensor array for q-PCR reaction utilizing three-metal PCB technology, *Sensors and Actuators B* 2014; 204:459-66.

connected to external instrumentation through solderable pin holes, showcasing reliable and convenient interconnections between devices and instrumentation. The miniaturized format of the prototyped device ensures its portability for POC diagnostics. The experimental results indicate the acceptable performance of the qPCR device to prior arts.

3.1. Introduction

Miniaturized biochips have emerged as important tools in the field of bioanalysis for many reasons, including the potential for portable point-of-care diagnostics using small reagent volumes. One important bioanalysis, quantitative polymerase chain reaction (qPCR), is a well-established and standard molecular technique to amplify, detect and quantitatively analyze nucleic acids in biological species of interest through thermal cycling. Micro-devices for qPCR have been widely studied, with current trends aiming to develop them with feasibility for mass production, simplicity of system integration, and low cost per measurement [6,27]. These requirements lead to electrochemical approaches that feature stability, low cost, and the possibility for use in disposable devices. Electrochemistry-based detection methods for qPCR have been widely investigated as options to improve poor portability of bulky fluorescence-based instruments [28-30]. Electrochemical intercalator based methods using redox indicators, such as methylene blue (MB) and ferrocene, have been suggested in these investigations. Luo et al. also reported a new approach using specially designed and synthesized ferrocene-labeled peptide nucleic acid probe, which was expected to minimize false-positive results [31]. However, prior research has focused primarily on monitoring the interactions of the chosen redox indicators with the PCR product, while still utilizing conventional thermal cyclers that are not portable [28-31]. Alternatively, others have developed systems that combine flow-through heaters with micro-fabricated or commercial sensors to form microfluidic systems [32,33]. However, these systems require complicated microfluidic interconnection and apparatus to flow the solution back and forth between the heaters and sensor, leading to inconvenience for multiple samples and/or multiple analyses. Other researchers have proposed a PCR device that utilized a glass-based electrochemical biosensor, and a micro-machined chamber on one side of a silicon wafer with a heater that was patterned the other side. The electrochemical sensor and the chamber with the heater were attached

and sealed to form a PCR site [34,35]. The device utilized microfabrication techniques on materials such as glass and silicon, which led to problems of integration such as electrical interconnection with instrumentation and liquid control. In order to solve these problems with existing qPCR microfluidics, an integrated and electrochemical biosensor device for qPCR is proposed. The devices feature localized three-electrode voltammeters and thermal cyclers that can be formed easily into large arrays of individually addressable units with convenient system integration.

Electrochemical detection for qPCR is usually performed using three-electrode voltammetry [54-60]. Generally speaking, three-electrode voltammetry consists of a working, an auxiliary, and a reference electrode, and is a universal tool which is able to derive electrochemical information about an analyte in solution by measuring the signals from a redox reaction at the electrode interface as the applied potential is varied [36]. Noble metals, such as gold and platinum layers, are usually used as electrode materials that are deposited on silicon wafers by sputtering and photolithography processes, which may be unavailable in common laboratories and are associated with an increase in cost due to the need for specialized equipment and clean room microfabrication facilities [37]. In addition, metal thin films deposited via microfabrication processes such as sputtering are very vulnerable to scratch. Furthermore, silicon substrates don't allow secure electrical interconnection or facilitate system integration with other microfluidic components. In addition, screen-printed carbon ink has also been widely used as electrodes in devices such as glucose sensors for reasons of low cost; however, the composition of solvent in the ink significantly influences its electrochemical performance and restricts its application in some non-aqueous solutions [38].

Several recent studies have suggested the printed circuit board (PCB) as a new platform to improve practicality of general microfluidics functions, such as liquid control in microfluidic channels and digital droplet manipulation [39,40]. PCB platforms have also been suggested for applications such as cell lysis and nucleic acid extraction [9-12]. Based on the success of this prior work, an array of integrated and electrochemical biosensor devices for qPCR with localized three-electrode voltammeters and thermal cyclers utilizing three-metal printed circuit board technology have been developed. Through the use of electroless plating and photo-patterning, the metallic micro-electrodes on the printed

circuit board facilitate electrical interconnection with instrumentation and integration with microfluidic components. The advanced and mature printed circuit board technology ensures reliability, reproducibility, and low cost for mass production of both single device, as well as arrays of devices. In the proposed system, the metal layers were deposited on the board by electroless plating, and the electrochemical properties of the electrodes were investigated. Utilizing the proposed on-board technology, qPCR was demonstrated as an example of complex electrochemical biosensing with integrated thermal cycling. The objective of the work is to develop an array of electrochemical biosensors utilizing printed circuit board technology to facilitate industry-friendly processes that support the possibility in mass manufacturing of miniaturized lab-on-a-chip systems.

3.2. Material and Methods

The overall system consists of: (1) arrays of three electrodes made of gold and silver on the same planar surface on the front side of the board; (2) arrays of resistive heaters made of copper, which simultaneously act as temperature sensors, on the back side of the board; and (3) double-sided pin holes for electrical interconnection, forming an array of compact devices. The overall device design for a single device is shown in Figure 3.1f. In this section, the fabrication process to realize arrays of these devices, as well as the methodology used to test them, is presented.

3.2.1. Fabrication Process

The overall fabrication process is shown in Figure 3.1. Electroless plating, which is an auto-catalytic chemical technique, was used to deposit layers of metal on 254-μm-thick fibreglass epoxy sheets (FR4, Ventec). The electroless plating process enables a wider range of film thickness and is simpler than sputtering; it was achieved by the process of reactions between a reducing agent with metal ions on the metallic substrate and non-conductive substrates after surface pre-treatment and activation [41-44]. Multiple layers of different metals were formed through processes involving several immersions into chemical baths in an automatic production line. As shown in Figure 3.1, after the pin holes were drilled, the FR4 sheet was cleaned with monopersulfate and peroxide based microetch (Oxone® PS-16, DuPont) and immersed in colloidal palladium-tin catalyst (CataprepTM404 and CatapositTM44, Dow). A 2.5-μm-thick copper thin film was deposited on the board by an electroless plating kit that mainly contains copper sulfate and formaldehyde as a reducing agent (CircupositTM3350 and CupositTM, Dow). The copper thin film was then patterned by dry film photolithography (Riston®, DuPont) and copper etching in ammonium persulfate (High Speed AC-CU guard Plus Replenisher, Phibro-Tech). The copper film on the front side was prepared as a seed layer for gold plating to form the microelectrodes, and the film on the back side was patterned into a serpentine pattern with a wire width of 130 μm to form a resistive heater for each device. To deposit gold only on the working and auxiliary electrodes, a dry film photoresist was photo-patterned again to cover up the reference electrodes. The board was then cleaned, pre-dipped into hydrogen chloride, and activated by another palladium catalyst

(Ronamerse SMT Catalyst, Dow). Nickel was plated (DurapositTM SMT 88, Dow,) as an adhesion layer followed by plating of 6-μm-thick film gold (AurolectrolessTM 520 SMT, Dow). A clear photo-imaging solder mask (LPISM) (PSR-4000, Taiyo) was screen printed, patterned, and cured to protect each heater and circuit except in the areas of the microelectrodes and pin holes. Prior to silver deposition on the reference electrodes, another dry film was applied and patterned to cover the gold electrodes. The board was then immersed into a solution containing silver nitrate, allowing silver to be electrolessly plated on the reference electrodes (AlphaTM STAR, Enthone). After the dry film photoresist on the board was stripped, the Ag/AgCl electrodes were formed through immersion into 0.1M potassium chloride with 0.3 V across the silver electrodes and a platinum wire (as a counter electrode) for 12 hours. A 100-μm-thick SU-8 layer was finally coated and patterned to cover the board area only leaving the electrodes exposed to the air.

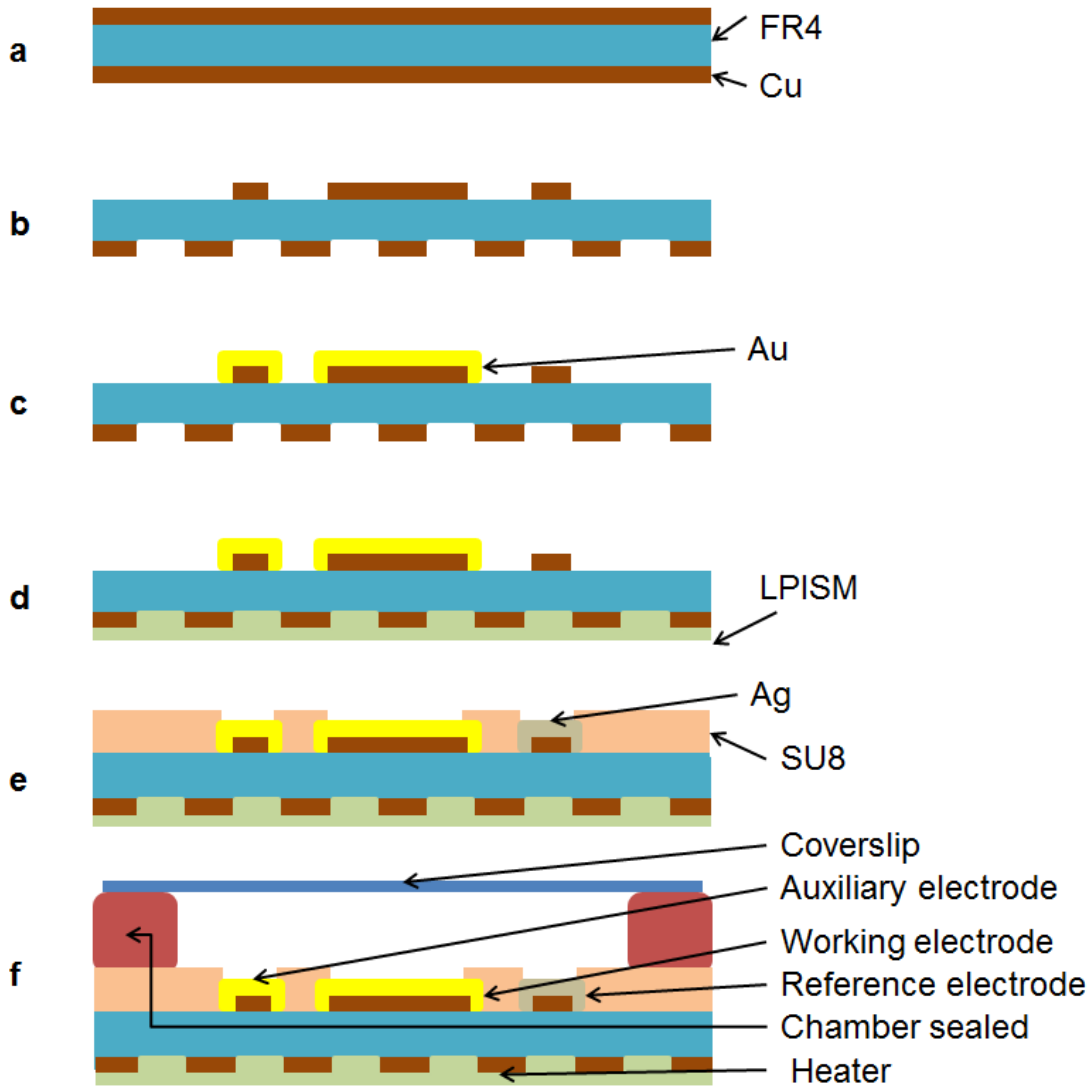

Figure 3.1. Fabrication process for arrays of devices containing biosensors and heaters (a single device is shown for simplicity): (a) Copper was electrolessly plated on FR4 substrate. (b) Copper layers were patterned to form the base for a three-electrode structure on the front and for a thermal cycler on the back. (c) Gold was selectively plated onto the working and counter electrodes. (d) Soldermask was applied to protect the heater on the back. (e) Silver was electrolessly plated on the reference electrode followed by SU8 coating. (f) The chamber was sealed, attached to the sensor, and covered by a glass slide, forming each biosensor on the board. (The figure is not to scale of the actual dimensions.)

3.2.2. Cyclic Voltammetry

A few previous studies have reported different electrical resistivity and surface morphology between electroless plated metals and bulk metals [45]. To validate the electrochemical properties of the fabricated electrodes, the roughness factor, which is the ratio of the electrochemical active surface area to the geometrical area [46], was estimated by the cyclic voltammetry method.

Cyclic voltammetry is a useful tool to obtain quantitative information, such as concentration, about a redox indicator in solution. During experimentation, the potential of a device's working electrode is usually scanned back and forth linearly with time in a range of interest. When the potential is more positive than that of a redox indicator in the solution, the indicator may be oxidized and produce an anodic current. Similarly, on the return scan, as the potential becomes more negative than the reduction potential, a cathodic current may be induced. The magnitude of the faradaic current depends on the rates of the several parameters. The expression of the peak current in a reversible system at 298 K is given by the Randles–Sevcik equation [47],

$$ip = 2.69 \times 10^5 \times \mathrm{n}^{3/2} \times \mathrm{A} \times \mathrm{D}^{1/2} \times \mathrm{v}^{1/2} \times \mathrm{C}$$

where *n* is the number of electrons exchanged during the redox process, *A* (cm^2) is the active area of the working electrode, *D* ($cm^2\ s^{-1}$) and *C* ($mol\ cm^{-3}$) are the diffusion coefficient and the bulk concentration of the electro-active species, respectively, and *v* is the voltage scan rate ($V\ s^{-1}$). If all other parameters in the equation are known, the active surface area of the working electrode can be estimated. For our work here, at least three sensors from different arrays were randomly chosen from each of two printed circuit board panels in order to test and validate the variation between electrode samples. The electrodes were tested by a cyclic voltammeter (AFC-BP1, Pine Bipotentiostat), which was controlled by computer software (ASTP-B01 Module Aftermath Scientific Data Organization). For each device, the circular gold electrode, rectangular gold electrode, and a silver/silver nitride (CH Instruments) electrode were connected to the voltammeter to act as working, counter, and reference electrodes, respectively. For the surface area estimation, 0.1 M of tetraethyl ammonium perchlorate (TEAP) (Sigma-Aldrich) was prepared in acetonitrile (CH_3CN) (HPLC grade, Sigma-Aldrich) to serve as background

electrolyte for the final solution of 1 mM ferrocene ($Fe(C_5H_5)_2$) (Sigma-Aldrich). For the prepared solutions, a series of voltammograms were recorded between 0 to 1000 mV for 3 cycles at each scan rate (50, 100, 150, 200 mV s^{-1}) to measure the surface area of the electrode on the proposed devices.

3.2.3. Quantitative PCR

A PCR protocol based on the interaction of methylene blue (MB) with PCR amplification product was established for this study. MB was selected for its simplicity and low cost, compared with other electrochemical methods using, for instance, Fc-PNA, which requires special probe design and synthesis leading to higher cost and more complicated experimental optimization. MB binds respectively with ds-DNA by intercalative binding and ss-DNA via free guanine bases [48,49]. In order to understand the nature of the redox indicator, MB, the cyclic voltammogram at different concentrations was obtained at 50 mV s^{-1} scan rate. Since the target DNA fragment number increases during PCR amplification, the concentration of free MB proportionally decreases due to consumption of binding and leads to lower peak redox current signal measured by the cyclic voltammetry through a three-electrode sensor. The peak redox current was obtained after the elongation step of PCR to monitor progress of the amplification and to determine the level of qPCR amplicon according to many similar investigations from other researchers [54-56]. In this work, varying concentrations of *Drosophila melanogaster* genomic DNA obtained by extraction from fruit flies [50,51] were suspended in a PCR buffer containing 50 mM KCl, 20 mM Tris-HCl, 2 mM Mg^{2+}, 0.2 mM dNTP mixture, 0.67 units Taq DNA polymerase (Invitrogen), 60 μM MB (Sigma-Aldrich), and a pair of primers (IDT) to amplify a 500 bp gene fragment. The sequence of the forward primer was 5'-CAG GAT CCA TGT TCC CCC ACT TGA AGG GC-3', and the sequence of the reverse primer was 5'-TCG AAT TCT CCA CAC TCA CAT CGC GGA AGG-3'. As shown in Figure 3.1f, to construct on-board PCR experiments, 1-mm-thick sterilized chambers (Grace Bio-Labs) were adhesively bonded onto the board to hold 20 μl of test solution, each covered by a 0.5-mm-thick glass slide, and 35 thermal cycles including denaturation (94 °C, 30 s), annealing (65 °C, 20 s), and elongation (72 °C, 40 s) temperatures of the sample were executed by the heaters in each tested chamber. At least three PCR experiments were executed and repeated using separate arrays of devices in which seven different initial

DNA copy numbers, 10^7, 10^6, 10^5, 10^4, 10^3, 10^2, and negative control, were allocated in each individual device of arrays. Comparison tests of the same sample species and initial DNA copy numbers using a commercial qPCR kit (Fast SYBR® Green Master Mix, Life Technology) were executed in an optical real time PCR system (Applied Biosystems StepOne™).

3.2.4. Thermal Cycling

The temperatures of the heaters were individually regulated by a programmable feedback control on pulse width modulation for joule heating of copper, where each resistive copper serpentine functioned not only as a heater but also a temperature sensor by frequently measuring the temperature dependent resistance of the copper heater with a circuit consisting of MOSFETs and voltage dividers. Voltage across and current flowing through each heater were both measured via a microcontroller (Arduino) to determine the resistance of each heater. These values were then converted to temperature readings via the known temperature coefficient, which was found to be 0.0041 K^{-1} (S.D. = 0.0005, n = 6) by two-point calibration using a k-type thermocouple. The system was able to support an array of 4 heaters to execute multiplexed temperature control. The heater system was controlled using a proportional, integral and derivative (PID) controller, which is a third order system, in order to have more control over the response of the uncollected temperature of the heater, while minimizing the steady state error.

3.3. Results and Discussion

3.3.1. Surface Morphology

A 2×2 array of three-electrode patterns and heater combinations is shown in Figure 3.2a. The layout of a single device with three-electrode voltammetry and thermal cycler is shown in Figure 3.2b and c. Three electrodes fabricated by the electroless plating were imaged by scanning electron microscope (SEM) (FEI/Aspex, Explorer). A closer view (× 500 magnifications) of the rectangular area in Figure 3.3a is shown in Figure 3.3b, where a slightly roughened surface was observed. To further estimate the surface area, surface topography of the electrode was scanned using an atomic force microscope (AFM) (AFM Workshop, SA-AFM). The results are shown in Figure 3.4a, which shows that the height of the surface roughness was measured to be 0 ~ 2.5 μm in a 40 × 40 μm scanned area. The surface area was further calculated based on the 3-dimensional topographic measurement of AFM using built-in software in the AFM system. The result indicates only a 3% difference (n = 3, S.D. = 1.1%) between the geometric area (1600 μm^2), and measured surface area taking roughness into consideration. The cross-sectional view of the circular gold electrode is shown in Figure 3.4b, indicating that the thickness of the gold layer is approximately 6 μm.

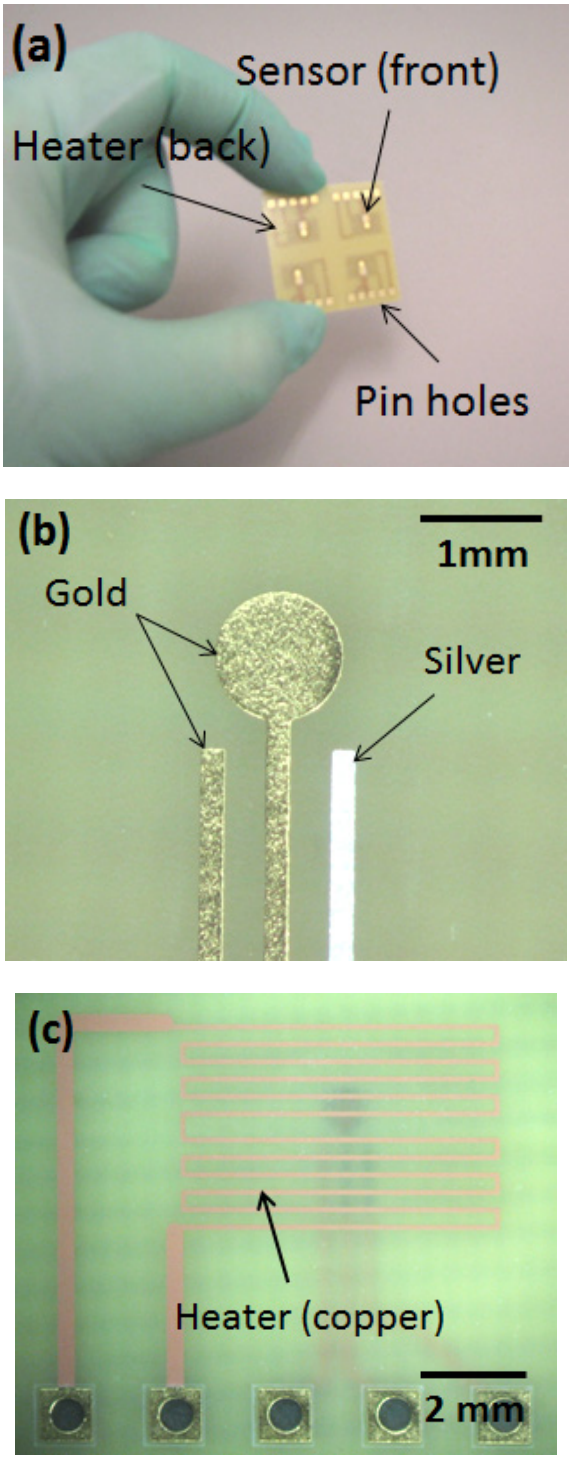

Figure 3.2. (a) Image of the 2 by 2 array of 4 devices (front). (b) Image of the three-electrode biosensor (front). (c) Image of the serpentine-shape thermal cycler (back).

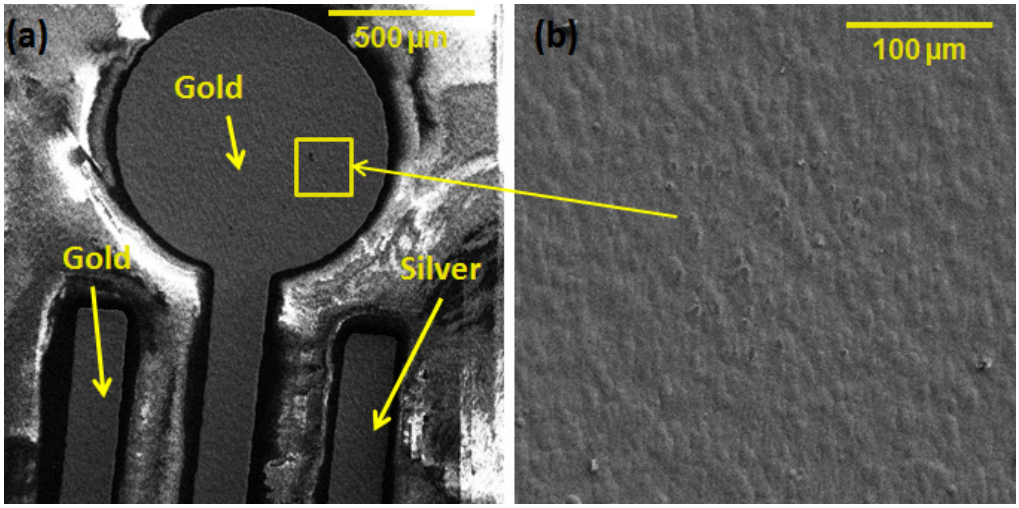

Figure 3.3. (a) SEM images of a single three-electrode sensor of gold, gold, silver (×100 magnification). (b) Close-up view of the rectangular area (×500 magnification) showing surface roughness.

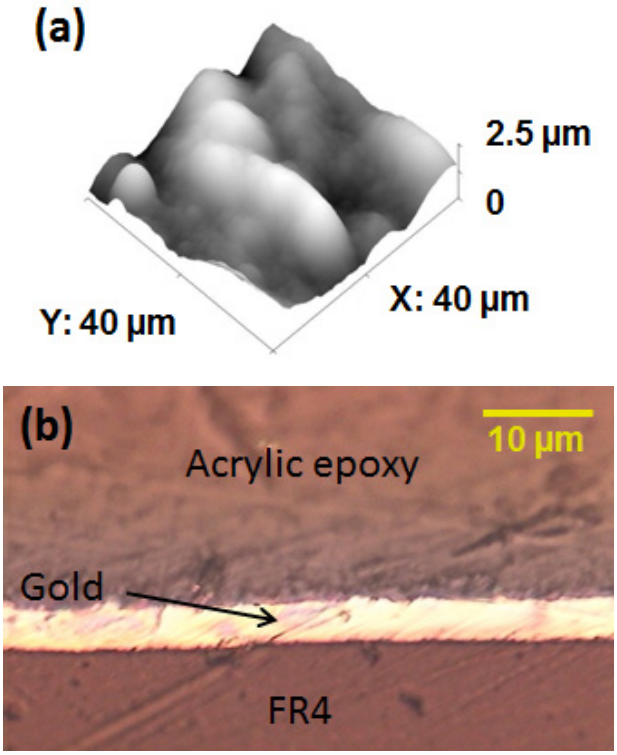

Figure 3.4. (a) AFM scan of the gold electrode surface. (b) Cross-sectional inspection of the gold electrode showing thickness.

3.3.2. Electrochemical Properties

To further derive the electrochemical active surface area of the working electrodes, cyclic voltammograms were obtained. The voltammogram (I-V plot) is shown in Figure 3.5a. As previous mentioned, the Rankes-Sevcik equation was used to solve for the active surface area by measuring the peak current with known parameters of *v*, *C*, *n*, and *D* (*D* can be found in the literature to be 2.53×10^{-5} $cm^2\ s^{-1}$ for the same chemical composition used in this study [52]). Results from four scan rates (200, 150, 100, 50 mV/s) were averaged and indicated that the average electrochemical active surface area of the tested working electrodes was 0.011 cm^2 (n = 15, S.D. = 0.004 cm^2), which is around one and half times the geometric area of the working electrodes as designed (roughness factor = 1.57). Compared with the result measured by AFM indicating no significant difference between geometric area and measured surface area, the result that the electrochemical active surface area is higher than the geometric area implies that the electrochemical active surface area of electroless deposited metals may own different surface properties than the bulk metals; however, this small difference may be due to the variation of the diffusion coefficient, which was derived from the literature. Assuming the surface area of the electroless plated metal is larger than that of the bulk metal, it is still not able to be asserted if the rougher surface results from the intrinsic electroless plating mechanism or from a non-specific fabrication setting deployed in the process. As shown in Figure 3.5b, the electrochemical performance of different electrodes is fairly consistent, indicating stable and uniform quality of the electrodes due to standardized manufacturing process in the PCB production line. It was noticed that the cyclic voltammogram produced noisier curves than those produced by characterization of the qPCR experiments. Possible reasons could be, first, the current signal level falls within the μA range for Figure 3.5, but the nA range for Figure 3.8 (in this case, around 10^2 times difference in scale). In addition, the experimental conditions were also set for totally different purposes. Furthermore, it is also speculated that the noise shown in Figure 3.5 did not come from the fluctuation of the current signal, but was due to the instability of the voltage output from the cyclic voltammeter (AFC-BP1, Pine Bipotentiostat) during the experiments.

In Figure 3.6, the relationship between the MB concentration (without DNA template) and the peak current of the cyclic voltammogram that is also shown in the figure

indicates that the peak current increased with the higher MB concentration in a non-linear trend. The slope of the relationship decreased at higher MB concentration with the slope transition at around 15-30 μM. The relationship between the MB concentration and the peak current of the voltammogram confirms the possibility of its use in qPCR.

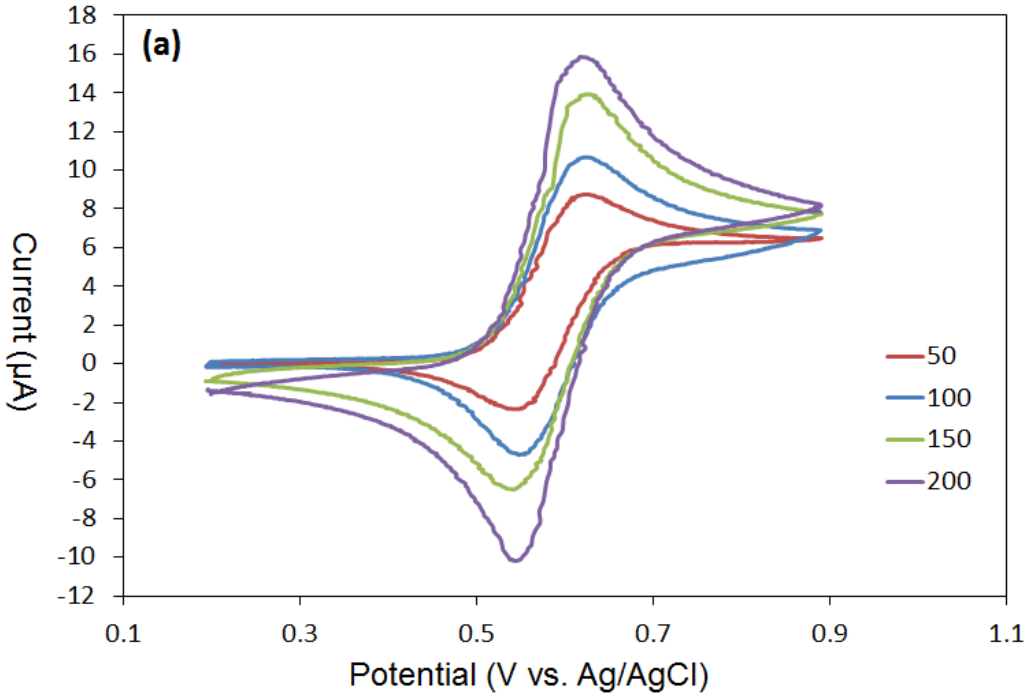

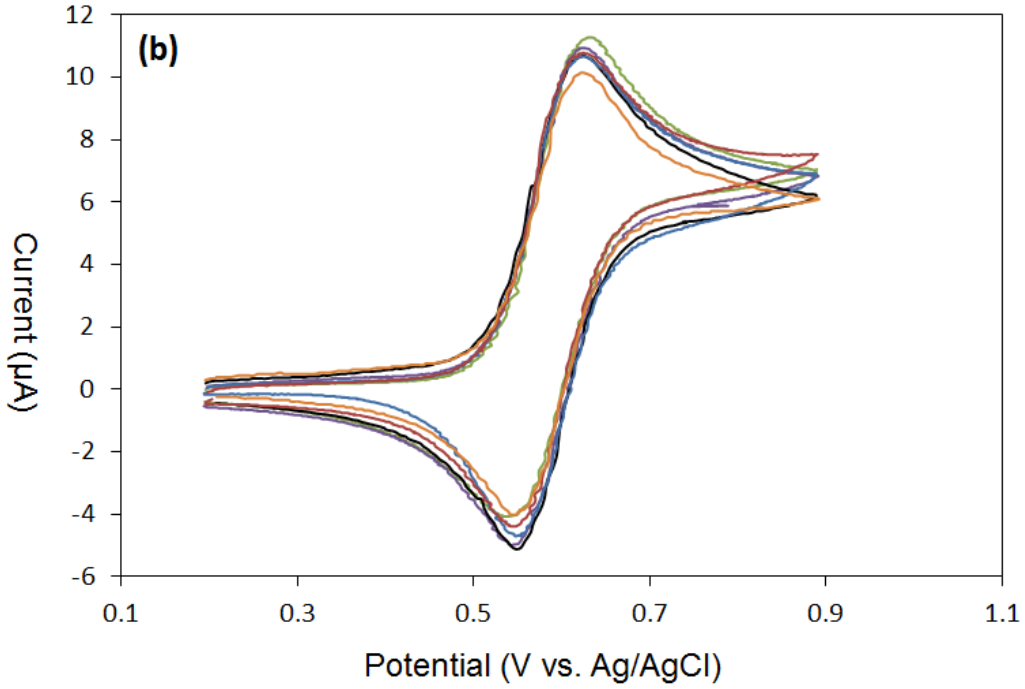

Figure 3.5. The cyclic voltammogram of 1 mM ferrocene and 0.1 M of tetraethyl ammonium perchlorate in acetonitrile: (a) at different scan rates (200, 150, 100, 50 mV s^{-1}); (b) at 100 mV s^{-1} from each three sensors from two different board panels (total six sensors).

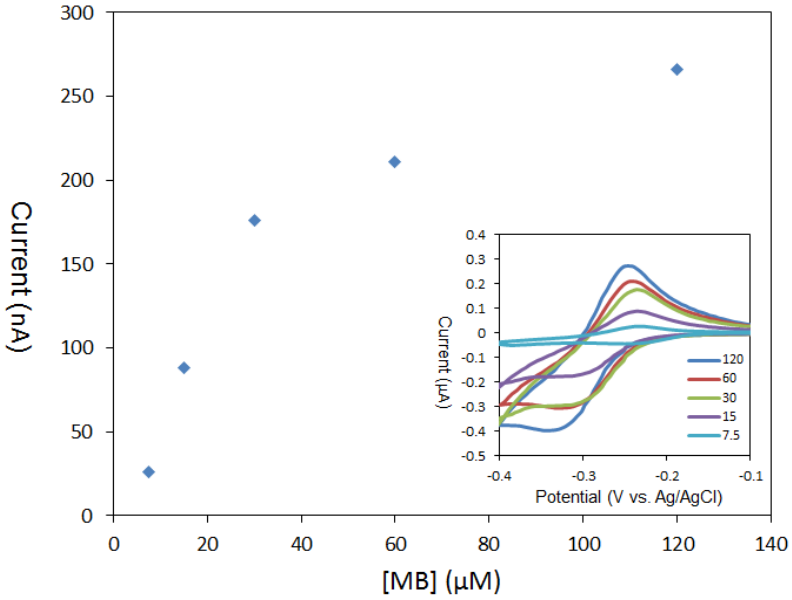

Figure 3.6. The relationship between the MB concentration and the peak current from the cyclic voltammogram (MB concentration: 7.5, 15, 30, 60, 120 µM; scan rate: 50 mVs^{-1}) shown at left corner as examples.

3.3.3. PCR Biosensor

PCR experiments were completed using integrated devices with three-electrode electrochemical sensors and thermal cyclers (Figure 3.1f). In Figure 3.7, the temperature profile of thermal cycling and holding between three temperatures from one heater is shown as an example. Figure 3.7 indicates that the on-board thermal cycler was able to accurately switch between each temperature promptly with little overshoot or fluctuation. A k-type thermocouple was attached on the board near the sensor (front side) to confirm that no significant temperature delay or difference (< 1 °C) was observed across the thin board. In order to take the possible temperature difference resulting from the 254-μm-thick board into consideration, the heater/temperature sensors were calibrated (two point between around 65 and 94 °C) from the sensor side in steady state for all experiments. To investigate the temperature gradient in the chamber, a technical difficulty was met in the attempt to measure the temperature profile across the chamber, especially the temperature near the glass slide. Specifically, the diameter of the thermocouple tip and wire were larger than the gap of the chamber. When they were inserted into the chamber, the sealing failed to hold the liquid and leaked. I also tried employing an infrared remote thermometer, but this was unsuccessful due to problems with scale mismatch between the thermometer and the miniature device, resulting in fluctuating values that were inconsistent. Therefore, I were only able to measure the temperature on top of the glass slide. The temperature was found to be around 3 °C lower than the temperature reading from the sensor. This temperature difference indicates a small temperature gradient vertically across the chamber. It was estimated that the temperature gradient across the 1-mm-thick chamber was around 2 °C, which might explain the slightly lower PCR efficiency in this study as the temperature could not be exactly set as needed for the different parts of the cycle. In the future, further improvements to the temperature uniformity should ensure a higher PCR efficiency; however, unless a hot lid is installed to form a closed environment such as is employed in conventional thermal cyclers; a temperature gradient would inevitably exist among most planar lab-on-a-chip systems.

In Figure 3.8a, the cyclic voltammogram of the MB-PCR mixture was carried out showing decreasing peak current at the 0, 25^{th}, and 30^{th} cycle due to less free MB molecules in the solution at higher cycles, which contained more ds-DNA, than at lower

cycles. In our quantitative PCR experiments, the potential values at which the peak signals occurred were observed to be around -0.22 V. The percentage decrease of these peak current values at different cycle numbers was then compared between varying initial DNA copy numbers as shown in Figure 3.8b. The PCR threshold cycle numbers (Ct) are the cycle numbers corresponding to the current signals decrease at 20 percent. It was observed that the higher the initial DNA concentration, the faster the peak current signal reached this threshold. The negative control confirmed low level of contamination. Note that the Ct values based on the 20% decrease in current signal are dependent on the initial concentration of methylene blue. To standardize for broad use, at least two tests with known initial DNA copy numbers should be done to calibrate the linear relationship between the PCR amplification and Ct for quantifying an unknown sample. In Figure 3.8c, by plotting the slopes of Ct values corresponding to the logarithm of various initial DNA copy numbers, and comparing these with the result using the commercial kit using an optical detection method, the PCR efficiency was calculated to be 102%. The PCR efficiency of the result from the electrochemical method using the proposed devices was calculated to be 95%, which is in the acceptable range for quantitative PCR. The detection limit of the electrochemical (MB) and fluorescence (SYBR® Green) method was respectively solved to be 59, and 1 initial DNA copy number by extending the slope line to find an intercept with the 35th cycle on the y-axis in Figure 3.8c. The results of a comparative gel electrophoresis experiment are shown in Figure 3.8d based on an example for initial DNA copy number of 10^5 and negative control. The overall results indicate that devices in the proposed array system were able to quantify amplification product of quantitative PCR.

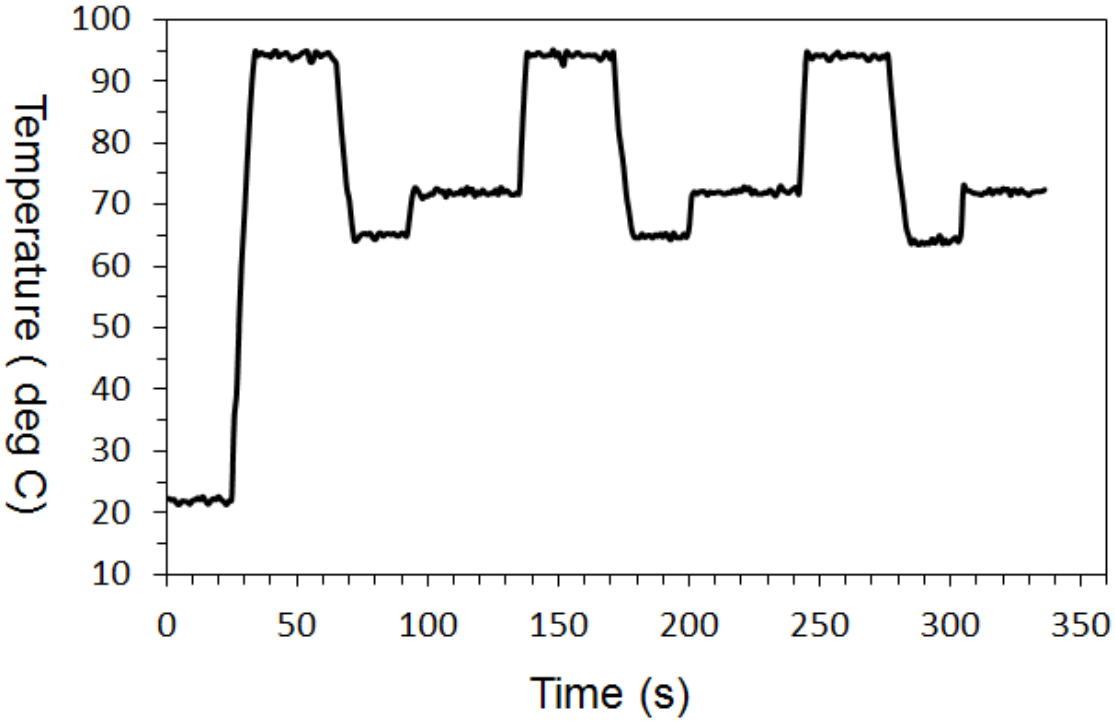

Figure 3.7. Temperature profile of thermal cycling for single example heater.

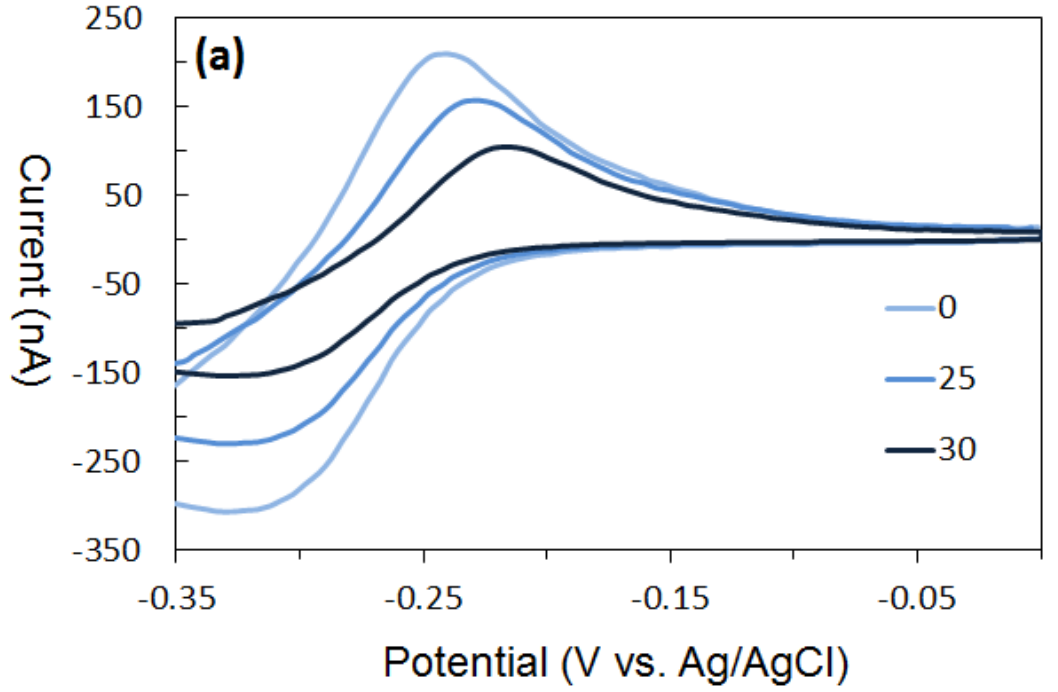
(a)
250
150
50
-50
-150
-250
-350
Current (nA)
-0.35
-0.25
-0.15
-0.05
Potential (V vs. Ag/AgCl)
0
25
30

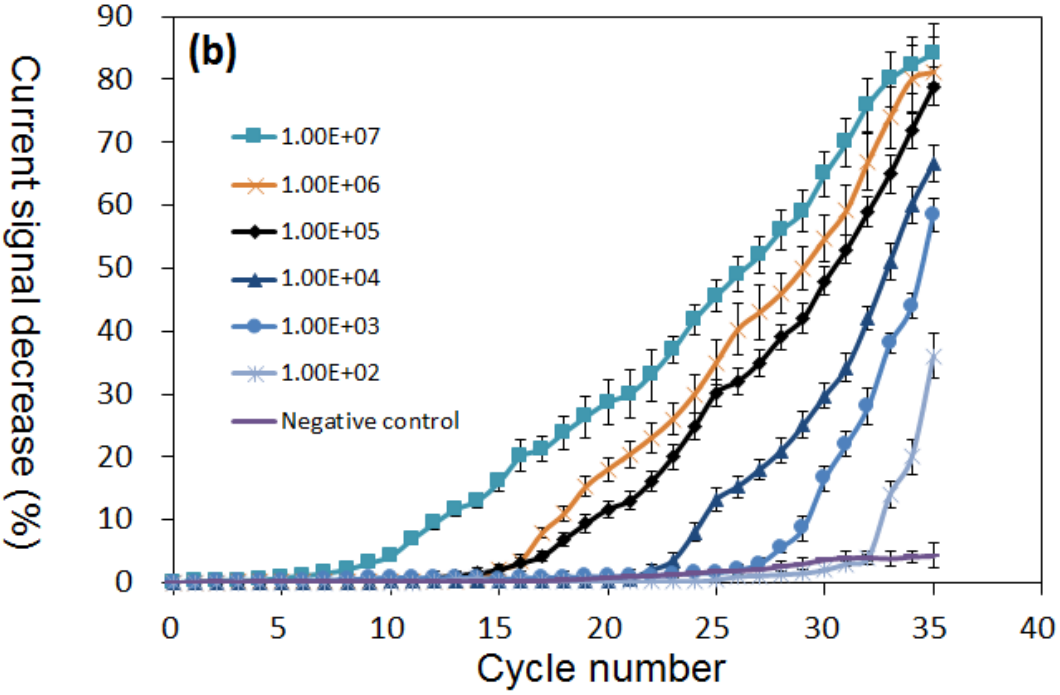
(b)
90
80
70
60
50
40
30
20
10
0
Current signal decrease (%)
0
5
10
15
20
25
30
35
40
Cycle number
1.00E+07
1.00E+06
1.00E+05
1.00E+04
1.00E+03
1.00E+02
Negative control

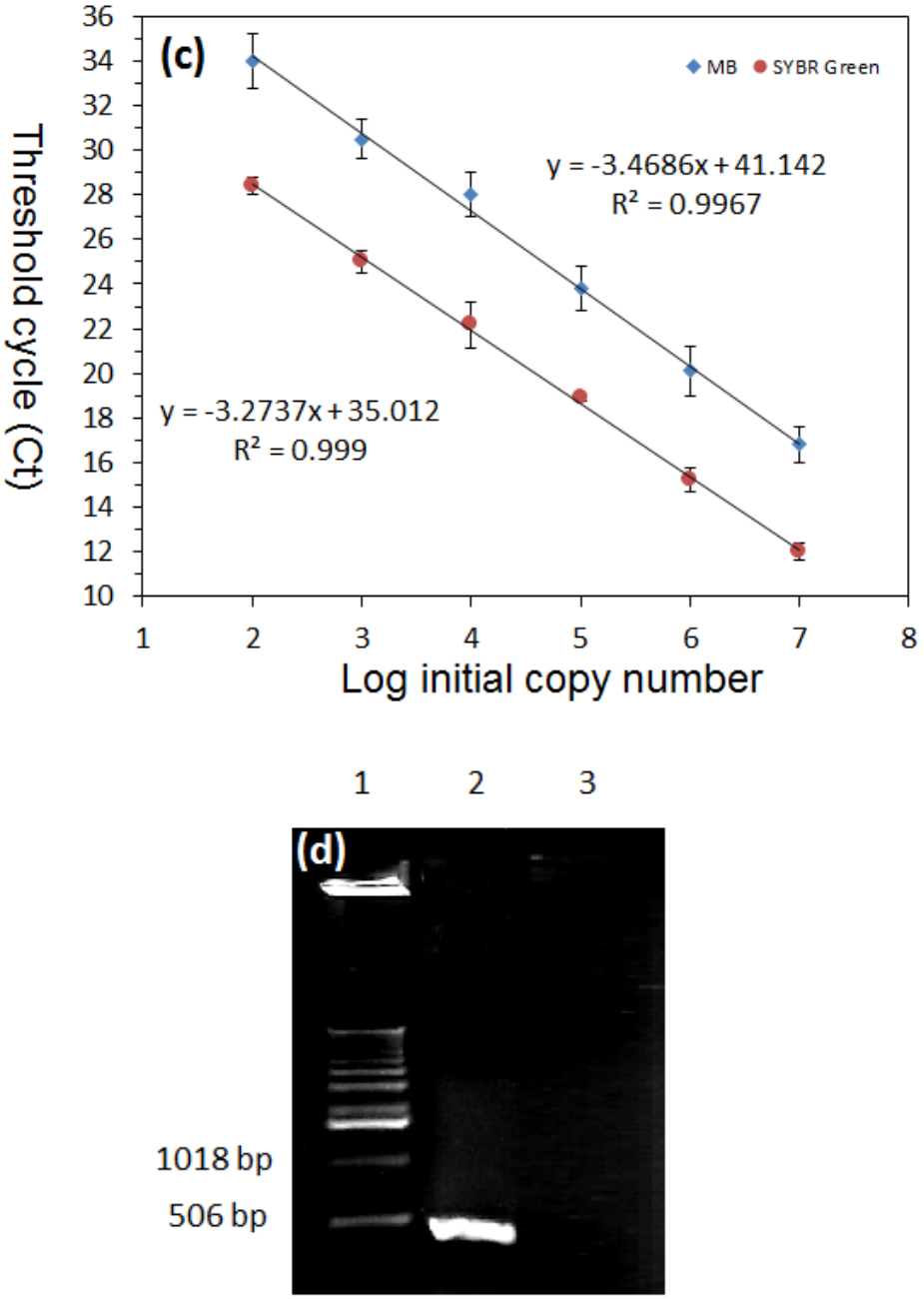

Figure 3.8. (a) The cyclic voltammogram showing the current signal of MB in PCR after 0, 25, and 30 cycles for initial DNA copy number of 10^5. (b) Percentage decrease of peak current vs. cycle numbers for initial DNA copy number of 10^7, 10^6, 10^5, 10^4, 10^3, 10^2, and negative control. (c) Ct vs. logarithm initial DNA copy number for experiments using MB and SYBR Green kit. (d) Image of gel electrophoresis showing a DNA ladder in lane 1, and the sample for initial DNA copy number of 10^5 and negative control respectively in lane 2 and 3.

3.4. Conclusion of the Work Presented in this Chapter

An array of electrochemical biosensors utilizing printed circuit board technology was successfully developed. Arrays of electrochemical biosensors and heaters were fabricated utilizing electroless plating deposition, where their electrochemical properties and surface features were investigated. An array of compact devices with electronic integration and automatic system was proven to be possible in this platform. qPCR using the proposed array system was performed as an example to confirm the system's capability in complex biosensing even though the sample loading method in this study is not the best for end-users, especially when large amount of experiments in arrays are conducted in places other than biological laboratories. In order to achieve a more user-friendly process of sample loading, microfluidic liquid control including reagents guiding and quantification should be designed and employed in the future before commercialization. This work suggests industry-friendly processes that support the possibility of utilizing printed circuit board technology in mass manufacturing of miniaturized lab-on-a-chip systems. It is believed that more investigation in the future on using the PCB technique for various applications of biosensing will be likely to facilitate the standardization of microfluidic components and propel the technology toward commercialization by rendering a platform of convenient system integration and a truly deployable tool for point-of-care diagnosis.

In this work, the prototyped array was made by automatic industrial manufacturing processes, showcasing industry-compatible standardized design and manufacturing processes. Biosensing elements (i.e. microelectrodes and heater) were fabricated for electrochemical measurement and thermal cycling, showcasing the integration of multiple functional units to achieve complex experimental conditions. All these components are connected to external instrumentation through solderable pin holes, showcasing reliable and convenient interconnections between devices and instrumentation. The miniaturized format of the prototyped device ensures its portability for POC diagnostics. The experimental results indicate the comparable performance of the qPCR device to prior arts.

Chapter 4.

On-board Array for Multiplexed Semi-active Cooling Rate Controlled Cryopreservation of Living Cells

An optimal cooling rate is a critical factor affecting the survival of biological cells during cryopreservation. In this chapter, a system for on-board cooling-rate-controlled cryopreservation under low-temperature (-80 °C) environments has been successfully developed with disposable, biocompatible polydimethylsiloxane (PDMS) storage chambers on top of localized heaters on printed circuit boards. The assembly allows the storage chambers to be removed from the temperature controlled board and transferred from a -80 °C freezer to a liquid nitrogen tank for long term cryopreservation. The use of PDMS enables the insertion of a syringe needle to load each sample, and during freezing, to seed extracellular ice formation. The PDMS storage chambers were fabricated using a polymethyl methacrylate (PMMA) mold made by a laser cutting machine. For each device, a copper thin film was deposited on a fiberglass epoxy substrate using electroless plating, and patterned by photolithography techniques into a micro-serpentine shape. The copper film functioned simultaneously as resistive heating elements and temperature sensors along with a PID feedback control program embedded in a microcontroller to semi-actively control the transient temperature profiles during the freezing process for multiple samples with different cooling rate requirements. The results show that our devices are able to maintain a stable cooling rate down to 1 °C per minute, which covers the optimal range for some mammalian cell types with low cell membrane permeability that low cooling rates are required. A heat transfer simulation was established to model transient and spatial temperature profiles of the device during the freezing. Preliminary biological tests on yeast cells and their survival rates after on-board cryopreservation imply that this prototype device can be a low-cost, reliable and convenient tool for laboratory use in cryopreservation. This work has been accepted by the Journal of Medical and Biological Engineering[3].

[3] Tseng HY, Malfesi S, Rahbar M, Tehranchi N, Jones J, Gray BL. On-Board array for multiplexed semi-active cooling rate controlled cryopreservation of living cells. *Journal of Medical and Biological Engineering* 2015; Accepted.

In this work, the heater boards and PDMS based chambers were made by automatic machining processes, showcasing industry-compatible standardized design and manufacturing processes. The array of heaters were fabricated using PCB technology for temperature control. The array of PDMS based chambers were fabricated by 3D printing and laser machining for sample loading. The developed array showcases the integration of multiple functional units to achieve complex design requirements. The heaters are connected to external instrumentation through solderable pin holes, showcasing reliable and convenient interconnections between devices and instrumentation. The miniaturized format of the prototyped device ensures its portability for POC bioprocessing. The experimental results indicate the outstanding performance of the rate controlled cooling to prior arts.

4.1. Introduction

Cryopreservation is a widely used technique adopted by various biomedical researches and clinical practices to facilitate activities, such as cord blood banking, artificial fertilization, and stem cell research [53]. Cryopreservation is based on the mechanism of diminished metabolism in a cell at cryogenic temperatures. To successfully achieve cryopreservation, the general process usually includes the addition of cryoprotectant agents to cells, cooling of the cells to low temperatures (-80 °C, dry ice temperature, or -196 °C, liquid nitrogen temperature at 1 atm), storage of the cells at these temperatures, followed by the warming of the cells and removal of the cryoprotectant agents from the intracellular environment of the cells. However, cells/tissues have been experimentally found to be damaged during low-temperature preservation. Among all the procedures, lethal injuries to cells is most likely to occur in the temperature region from -15 °C to -60 °C during the freezing and thawing processes [54,55]. When cell suspensions are being frozen, extracellular ice forms spontaneously or by seeding between -5 °C to -15 °C, whereas intracellular environment remains supercooled due to the protection of the plasma membrane from extracellular ice crystal growth. The rise of solute concentration in the surrounding media therefore induces a chemical potential gradient between the unfrozen intracellular and frozen extracellular environment. To equilibrate the potential difference the cytoplasmic water flows out through the plasma membrane causing cell

volume change. The physical behavior and survival rate of cells in cryopreservation highly correspond to cooling rates. When the cooling rate is too high, intracellular ice forms and irreversibly damages cell organelles [56,57]. Conversely, when the cooling rate is too low, cell shrinkage leads to excessive dehydration [58,59]. The two-factor hypothesis from Peter Mazur indicates that optimal cooling rates should be low enough to prevent intracellular ice formation, but high enough to avoid excessive shrinkage [60]. The optimal cooling rates of different cell types vary remarkably due to their distinct cryobiology characteristics [61]. Cell types with low optimal cooling rates (< 10 °C/min), such as hematopoietic stem cells [53,62], immune cells [63,64] and mammalian ova [65] require much more careful treatment than those with high optimal cooling rates (>100 °C/min), such as red blood cells [66] during their freezing processes to ensure maximal survival rates.

In practice, cell suspensions are stored in commercial cryogenic vials, and the cooling rate inside the vials can be high (>30 °C/min) during freezing. To achieve the low optimal cooling rates for certain cell types, researchers often use Styrofoam boxes or alcohol chambers to increase the thermal resistance between samples and a -80 °C freezer or liquid nitrogen [62]. However, the temperature and cooling rate of samples during freezing cannot be recorded in this setting. Users have to adjust the thermal insulation for desired cooling rate requirements by guessing and therefore accurate cooling rate controls are not guaranteed by these passive methods. Commercially available rate controlled freezers are considered to be the most reliable equipment in clinical applications. However, they are only affordable to few organizations because of their huge size and high cost. Additionally, these commercial units are not suitable for preserving precious small-volume samples or multiple samples with different cooling rate requirements at the same time. Li, *et al.*, proposed an on-chip cryopreservation of living cells in a device containing a microfluidic chamber and a heater made of indium tin oxide on glass to monitor the temperature of the samples during freezing [67]. However, an open-loop, instead of a closed-loop control process on the heater led to the non-linear and inconsistent freezing curves of temperature. In addition, electrical interconnections and the operation of wet processes in their design are not user-friendly due to the brittle glass substrate and microfluidic liquid control. To solve these problems, a simple, low-cost and automatic system is presented to semi-actively control the local cooling rate of samples in

conventional freezers. The on-board cryopreservation used an array of storage chambers sitting on localized elements that acted as both a heater and a temperature sensor, which were fabricated by printed circuit board (PCB) technology, to achieve desired cooling rates controlled by a USB powered microcontroller. The disposable storage chambers ensure low cost, simple operations and flexibility in a small sample volume. A copper thin film was deposited and patterned into an array of serpentines to act as the localized heating and temperature sensing elements that monitor and affect the sample temperature during cooling processes. The temperature sensing capability of the heaters eliminates the use of a thermometer and ensures simple packaging. The PCB manufacturing enables convenient electrical interconnections and standardized fabrication with the potential toward mass production. The closed-loop control instrumentation allows accurate and versatile cooling rate control with low power consumption and simple experimental setup. Our initial design combined various tools, functional units, materials and processes to form a compact prototype. It is presented as a proof-of-concept work, featuring its user-friendly integrated configuration, industrial-friendly manufacturing, and multi-functional system.

4.2. Material and Methods

4.2.1. Storage Chambers

As shown in Figure 4.1a and b, the storage chambers were made of disposable and biocompatible polydimethylsiloxane (PDMS). To form the chambers, the PDMS wells were cast, cured, released and cut from a Polymethyl methacrylate (PMMA) mold. The molds were fabricated by a CO_2 laser cutting machine controlled by Retina Engrave software (Full Spectrum Laser, USA). The PDMS chips were bonded onto a scotch tape strip coated with a PDMS thin film after sterilization, forming chambers, each with a volume capacity of 100 µl (inner diameter: 7 mm, inner height: 3 mm, thickness of chamber wall: 2 mm). The chambers were then adhered onto the board. A metal needle was inserted into each chamber as a seeding site to allow extracellular ice formation near -6 °C due to its direct contact with the surrounding low temperature. The self-sealing feature of PDMS allows sample loading using syringe needle injection, yet still provides an enclosed chamber after needle extraction. When the temperature of samples reached -80 °C in the freezer (Figure 4.1d), the chambers can be detached from the board and transferred to the liquid nitrogen tank for long term storage.

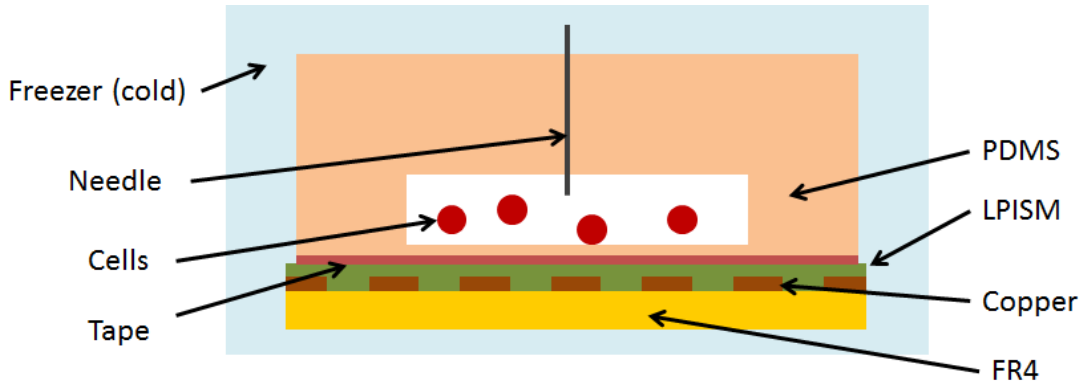

(a)

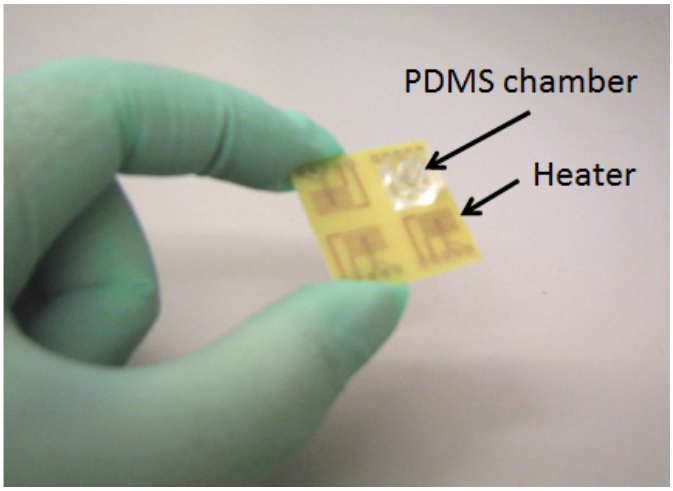

(b)

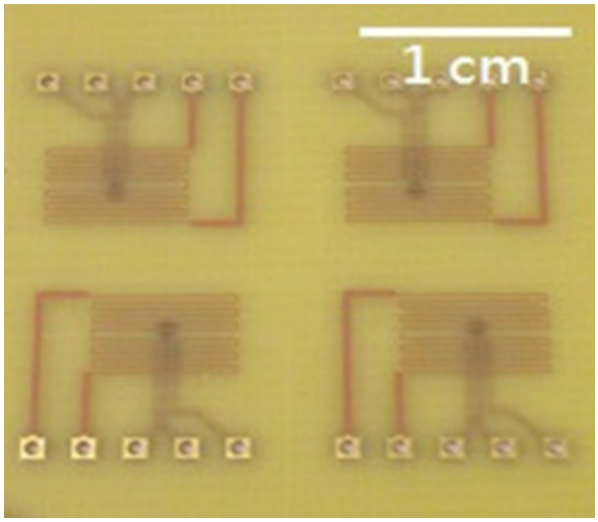

(c)

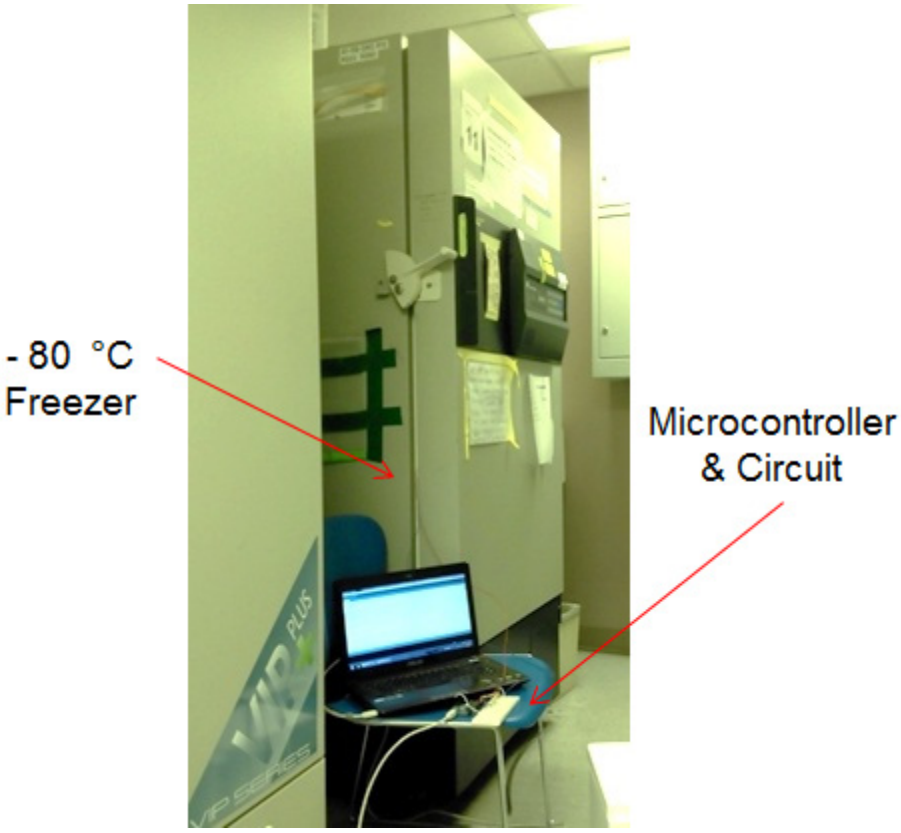

(d)

Figure 4.1. Demonstration of (a) overall device (PDMS: polydimethylsiloxane, FR4: fiberglass epoxy, LPISM: Liquid photoimageable solder masks), (b) one chamber on the board with four heaters in an array; (c) array of heaters in a close-up view; (d) experimental setup showing a USB powered microcontroller, a circuit, and a device as shown in (b) placed in a -80 °C freezer.

4.2.2. On-board Heating and Temperature Sensing Elements

The heater board acted as a substrate and was responsible for generating heat in a localized area to limit heat dissipation from the sample to the cold surroundings. The heating element also acted simultaneously as a temperature sensor by measuring the temperature dependent resistance of the copper thin film. The matured PCB technology was used to build platforms that contained heating and temperature sensing elements and electrical interconnections. In Figure 4.1c, the heating element is shown, which was fabricated with electroless plating and photolithography. After the pin holes were drilled,

the 250-μm-thick fiberglass epoxy (FR4) substrate was cleaned with monopersulfate and peroxide-based microetch (Oxone® PS-16, DuPont) and immersed in colloidal palladium-tin catalyst (Cataprep™ 404 and Cataposit™44, Dow). A 2.5-μm-thick copper film was deposited on the board by an electroless plating kit that contains copper sulfate and formaldehyde as a reducing agent (Circuposit™3350 and Cuposit™, Dow). The copper thin film was then patterned into an array of serpentines by dry film photolithography (Riston®, DuPont) and the copper etching of ammonium persulfate. As shown in Figure 4.1a, liquid photoimageable solder masks (LPISM, Taiyo) were finally coated to protect the heaters on the board. The resulting narrowest width of the heater wire was 130 μm, and the overall dimension rendered the resistance of the heaters to be around 12 Ω as measured by a multimeter. Note that the resistance of the heaters was designed to be exactly this point. Theoretically, a current of 340 mA through the heater would generate 0.1 watt of power. To generate the same power level, heaters with a lower resistance would require a larger current through the heater; those with a higher resistance would lead to a large voltage across them. Both cases are not desired for the USB powered microcontroller with a limited voltage- and current-output range. The manufacturing of the electroless plating is therefore necessary to produce the thin film copper, ensuring the intermediate resistance of the heaters. Practically, the power of joule heating was regulated by adjusting pulse width modulation using a programmable feedback control.

4.2.3. Instrumentation

The resistive copper serpentine functions not only as a heater but also a temperature sensor by frequently measuring the resistance of the heater. As shown in Figure 4.2, the circuit consists of MOSFET devices and voltage dividers (R6). Voltage across each heater and current flowing through each circuit were measured by the analog-to-digital pins of the USB-powered microcontroller (Arduino) to determine the resistance of each heater (RH1-RH5). This value was then converted to a temperature reading. The sampling period was chosen to be between 1 and 10 Hz. The system is able to support an array of 5 heaters to execute multiplexed cooling rate control. The heater system was controlled using a PID controller, which is a third-order system, in order to have more control over the response of the temperature of the chamber, while minimizing the steady state error [68]. The PID controller was implemented on the microcontroller which

calculated the proportional, integral and derivative terms as described in equations (1), (2), and (3),

$$P = Kp \times (T\ target - T\ current) \quad (1)$$

$$I = \sum Ki \times (T\ target - T\ current) \quad (2)$$

$$D = Kd \times (T\ last - T\ current) \quad (3)$$

$$Duty\ Cycle = P + I + D \quad (4)$$

The PID controller uses three terms to calculate the next value to set the heater to. The proportional term, Kp, multiplies the current error that is the difference between the current value and the target value. This term aims to minimize this error and a larger Kp will respond faster. The derivative term, Kd multiplies the difference between the last value and the current value and will slow down the response. This is done to avoid overshooting the target and creating oscillations. The integral term, Ki multiplies the sum of all the errors. This term adds some momentum to the system so it takes a little longer to slow down, and will remove any steady state error. Empirically the values of Kp = 100, Kd = 1, and Ki = 1 were found working well enough for our purpose. The frequency of the pulse width modulation signal was chosen to be 500 Hz and applied across the gate of each MOSFET transistor and was set as the sum of the three terms shown in equation (4). Note that the digital to analog converter had an 8-bit dynamic range, which the final control value was constrained to. The error sum of the integral term was also constrained to ±200 degree, to avoid it dominating the response and creating large oscillations. The large Kp was chosen because the system was desired to prioritize responding quickly and were not worried about briefly overshooting or oscillations that would die out on the time scales being interested in. A more detailed analysis of the impulse response of the system would lead to finer tuning of these constants and a more ideal response; however, this would not substantially change the results on the time scale of seconds.

To test the performance of the cooling rate control, a simple experimental setup in Figure 4.1d shows that the device was placed in a -80 °C freezer (Forma™ High-Performance Lab Freezers, Thermo Scientific) and connected to the external instrumentation consisting of the USB powered microcontroller and circuit. The temperature readings were processed by the instrumentation and displayed in a laptop computer. The experiments were executed in the Department of Molecule Biology and Biochemistry at the Simon Fraser University.

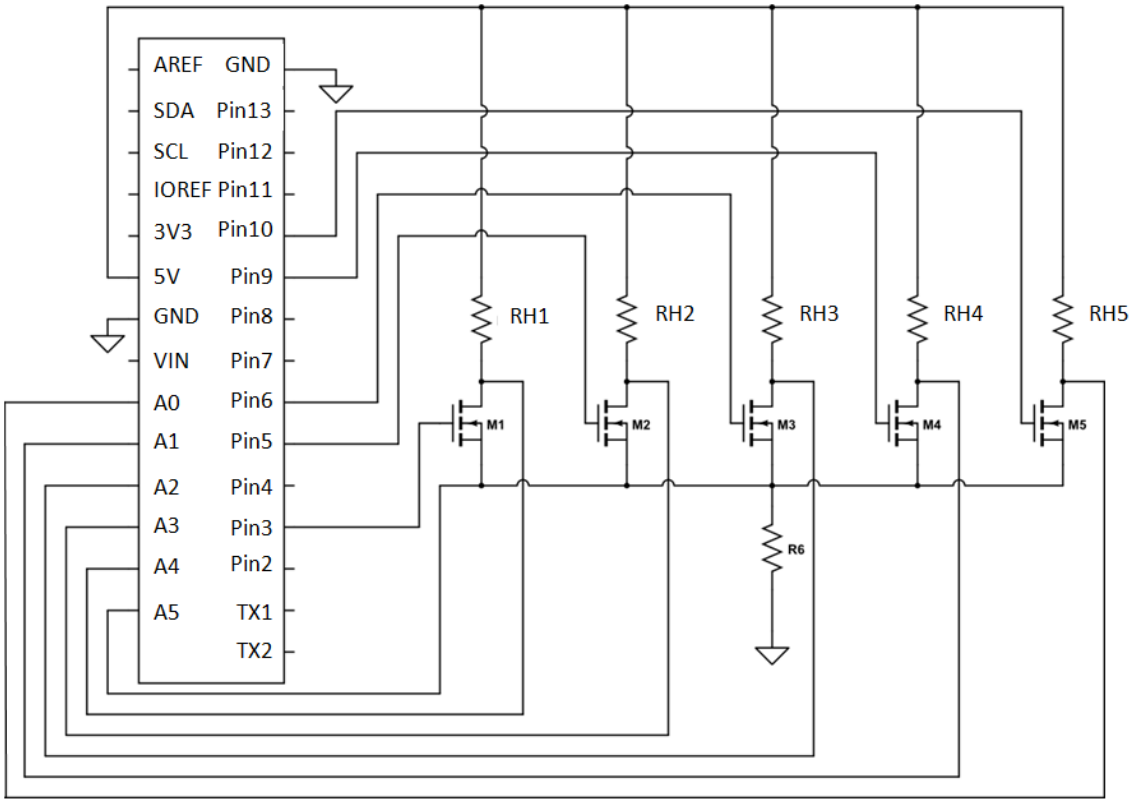

Figure 4.2. Schematic of the circuit and microcontroller for multiplexed temperature sensing and heating

4.2.4. Preliminary Tests on the Cryopreservation of Yeasts

Preliminary biological tests were also conducted using the fabricated devices. Yeast cells, *S. cerevisiae*, were cultured in conical flasks with 100 ml of medium (10 g/L of glucose, 3 g/L of pancreatic peptone, 3 g/L of yeast extract, and 1.5 g/L of Na_2HPO_4) by agitation at 25 °C for 65 hours. 1 ml of cell suspension was then centrifuged at 6000 rpm for 5 min and suspended in 1-ml distilled water. Two 100-μl cell suspensions were respectively loaded into the device and a conventional cryogenic vial. A controlled cooling rate of 5 °C/min was set for the experiments using the device, compared with those tests using the cryogenic vials and being placed into the -80 °C freezer without any cooling rate control. The cell suspensions were stored at the low temperature for 30 min before thawing. The cell suspensions were then taken out, plated in a medium supplemented with 15 g/L of agar in petri dishes, and incubated at 25 °C for 3 days. The viability measurements for the microorganisms were performed using the colony-forming unit (CFU) method by directly counting the colonies on the plates. The survival rates were derived from calculating the fractions with the colony numbers of the cryopreserved samples as numerators and those of the non-cryopreserved samples as denominators. Tests for the rate controlled cooling case and the non-controlled case were each performed three times.

4.3. Results & Discussion

4.3.1. Temperature Coefficient of Copper

Each resistive copper heater was used as both a heating and temperature sensing element. The temperature coefficient of resistance was measured by a high-end digital multimeter (Agilent, USA) throughout the test range of temperature (-70~20 °C). The actual temperature was measured by a k-type thermocouple with one decimal point resolution. The thermocouple was attached to the heater on the board at different temperatures to derive the relationship between copper resistance and temperature. As shown in Figure 4.3, the linear slope was converted to find the temperature coefficient, which was found to be 0.0041 K^{-1} (SD = 0.0005, n = 6). The reference resistance at room temperature (20 °C) was found to be 11.96 Ω. It can be seen in Figure 4.3, that the linearity was not perfectly maintained throughout all readings, and a maximal 4 °C variation was observed. These variations were influenced by the experimental setup more than the copper thin film itself, as the temperature coefficient of copper is a constant material property in this temperature range. The temperature coefficient of resistance should be determined and averaged by two-point calibrations for every new copper serpentine before its first time use. Based on the found temperature coefficient of resistance and the microcontroller with 10 bits of resolution, the accuracy of the resistive temperature measurements were found to be ± 0.5 °C, which is acceptable for cryopreservation purposes. As the part of conducting wires connected from the on-board interconnections to the instrumentation would be exposed to low temperatures, its error contribution was tested indicating that only a very minor change of resistance (0.25 mΩ/°C, SD = 0.04, n=3) was observed for a 30-cm-long wire.

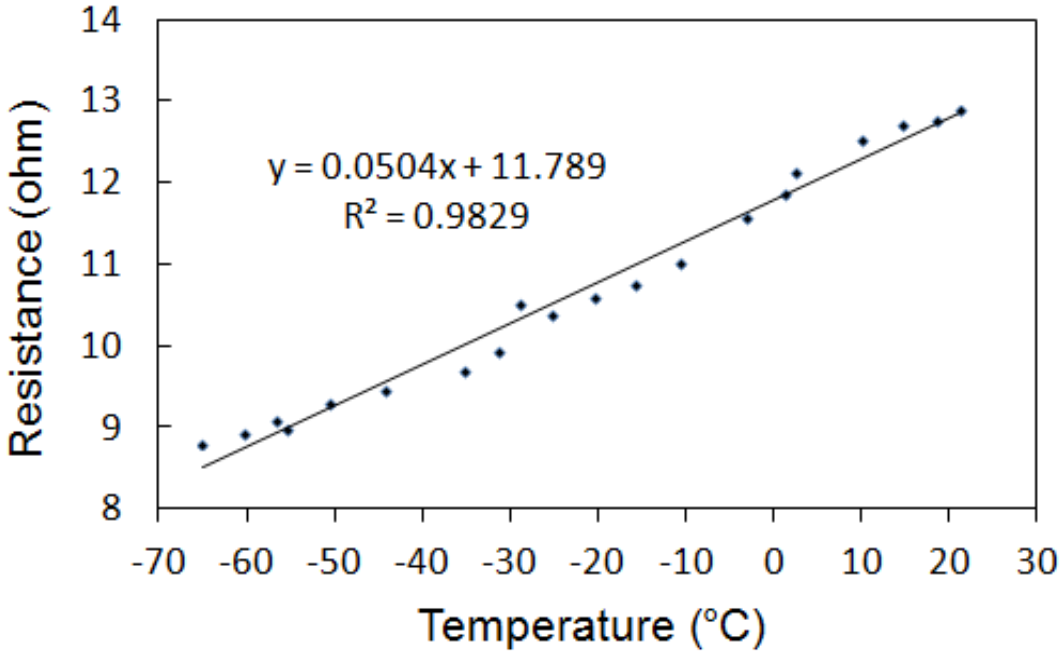

Figure 4.3. One example of the linear temperature dependency of copper thin film resistance

4.3.2. Cooling Rates

Since the chamber was designed to be adjacent to the heater with a thick insulation layer on its top, an assumption was made that the temperature reading from the heater represents the real temperature of solutions in the chamber. To validate the assumption, a thermocouple with thick insulation was inserted and securely attached to the bottom of the chamber to monitor the temperature difference, and that was less than 1 degree. To validate our system's capability and accuracy in cooling rate controls, three freezing curves were monitored with desired cooling rates set to be 5, 1 °C/min, and free falling (see Figure 4.4a). It was observed that the maximum cooling rate for the current chamber design is 30 °C/min, which is also adjustable by increasing or decreasing the thickness of the PDMS top layer. Note that a temperature rise was observed at -6 °C in Figure 4.4a (free falling) evidencing the latent heat release from the freezing of the liquid sample. The other two curves show that the low cooling rates can be maintained by this system. As shown in Figure 4.4b, a fast thawing rate (> 100 °C/min) was achieved by the heater in room-temperature air. In Figure 4.4c, a temperature holding at -10 °C was performed to

demonstrate the stability (± 0.5 °C) of temperature controls in the device. The system testing indicates its capability to monitor and control the temperature of samples during freezing and thawing.

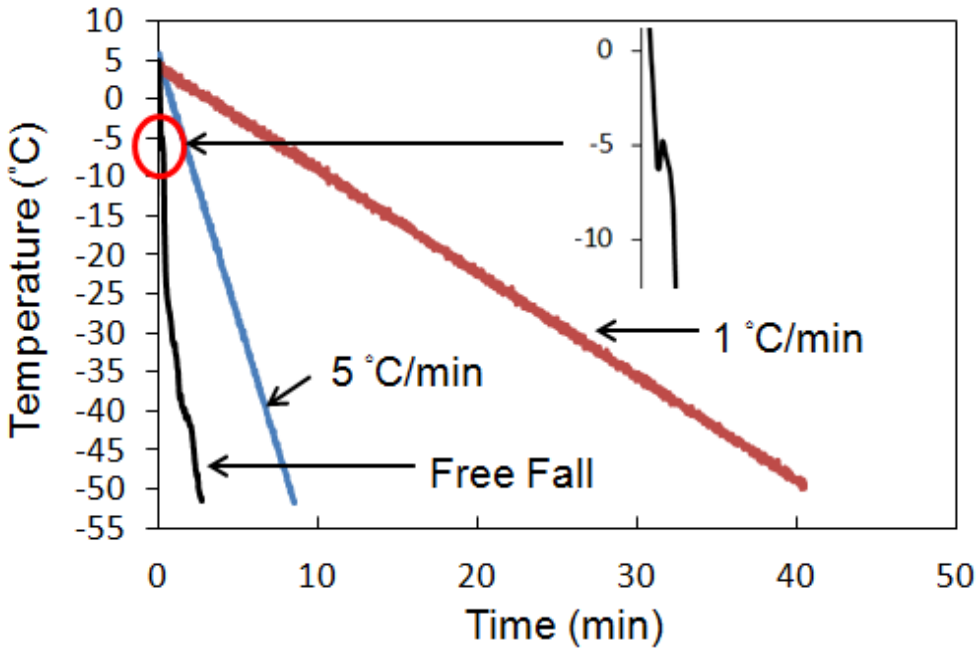

(a)

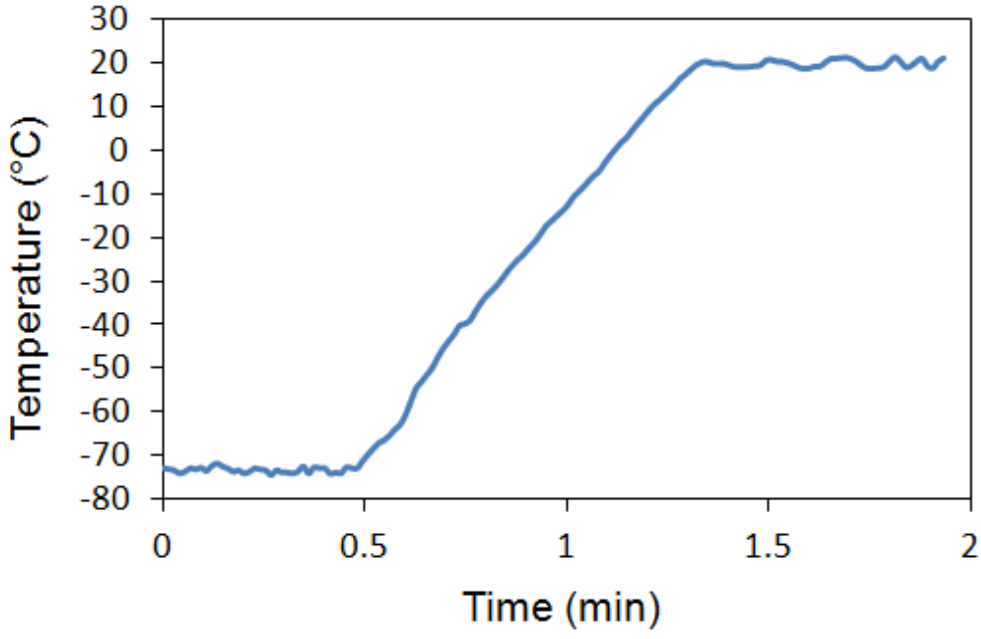

(b)

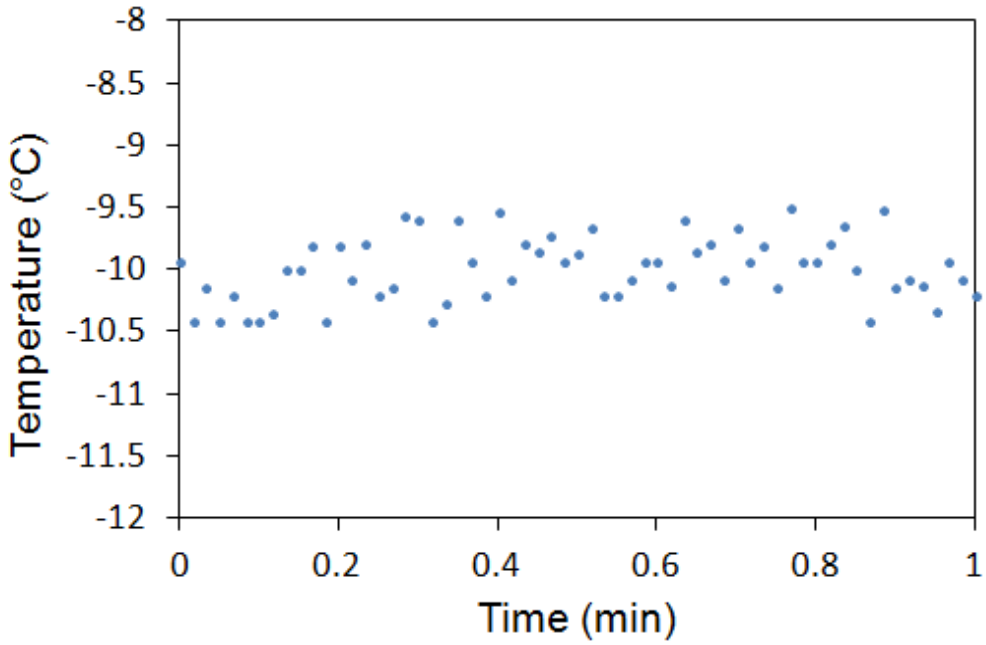

(c)

Figure 4.4. Transient temperature profiles of samples showing (a) freezing curves (left-right: free falling, 5, 1 °C/min; red circle: latent heat release), (b) rapid thawing, (c) holding at -10 °C

4.3.3. Spatial Temperature Profile in the Chamber

It was expected that temperature differences would exist across the top and bottom of the samples in the chambers. In order to obtain the temperature at the top of the chamber, a thermocouple with a thick thermal insulated wire was tried; however, the thick wire was not able to securely stay at the position. I instead tried to use a thinner thermocouple; however, in practice, the thermocouple was not able to reflect the actual temperatures as the extreme cold environment absorbed heat through the conducting wire from the thermocouple head. An infrared thermometer was not able to measure the temperature through the chamber wall. To further study the temperature distribution of the device, a two-dimensional simulation was established using the COMSOL Multiphysics software *heat transfer in solids* module. Input parameters, such as thermal conductivity, heat capacity, and density were used based on the material properties of PDMS (chamber wall), water (liquid sample), and fiberglass (board). The initial conditions of temperature

were set to be 20 °C for the device. A varying boundary condition modeling the cooling rate of 5 °C/min was applied to the heater on the board, and a convective heat flux at the outer surface of the device (free convective heat transfer coefficient, h = 20 W/(m^2-K) for air [69]) was set to be -80 °C . The solution was solved transiently from 0 to 1200 s with 100 s intervals. As shown in Figure 4.5a, the spatial temperature distribution at different time frames was obtained. The cross-sectional temperature distribution was displayed in Figure 4.5b. The largest temperature gradient can be roughly seen at the third line from the top showing that the temperature difference between the top and bottom of the sample falls in a 10 °C interval (270-280 K). Temperature values at the top and bottom of the sample were extracted using the point evaluation in COMSOL, indicating that the vertical temperature gradient across the liquid sample in the storage chamber (3 mm height) reaches the maximum (< 8 °C) in the early stage of the cooling process, whereas a minor temperature gradient was observed in the rest of time. The result indicates a uniform temperature distribution of samples in the chamber throughout the lethal temperature range for cryopreservation from -15 to -60 °C.

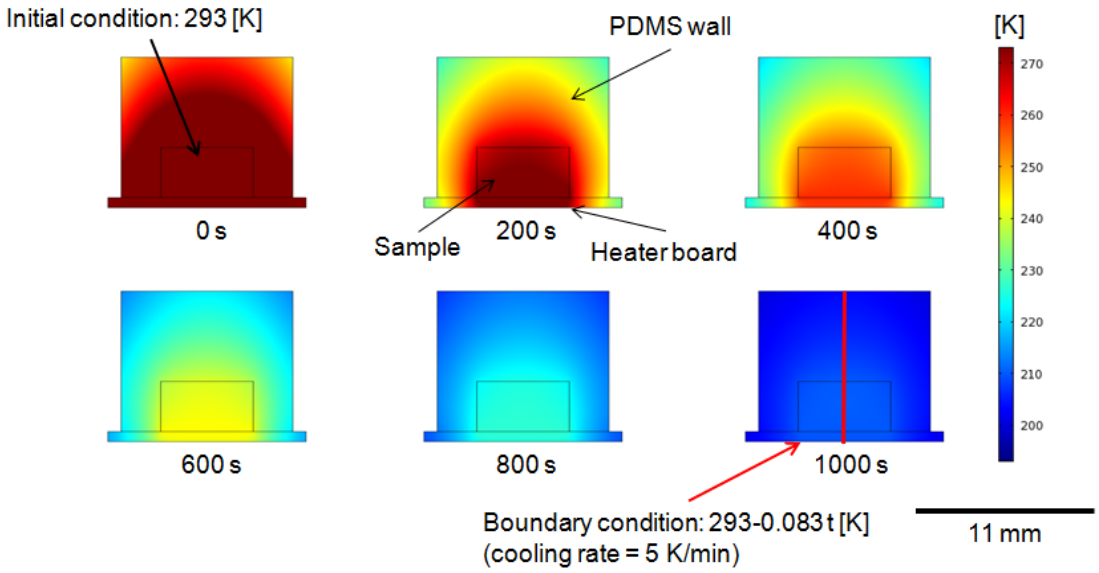

(a)

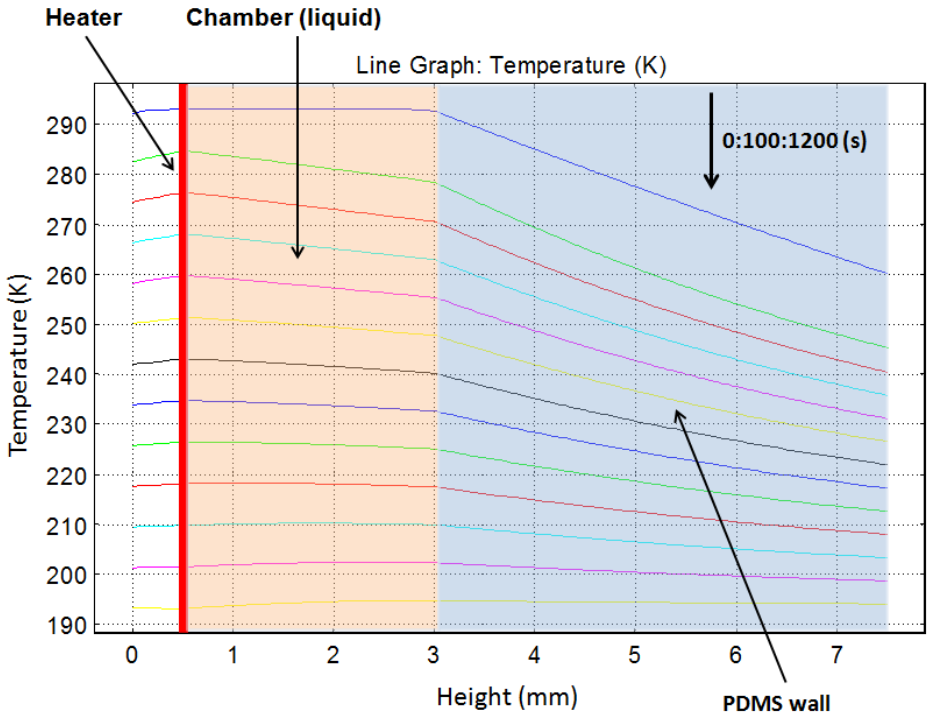

(b)

Figure 4.5. (a) Spatial temperature distribution of the device in low temperature environment at different time frames, (b) Cross-sectional spatial temperature distribution (red line in (a), 1000s) at different time frames

4.3.4. Survival Rate of the Yeasts

The preliminary results from the simple biological tests imply that the on-board cooling-rate controlled cryopreservation could improve the survival rates of the cells. As shown in Figure 4.6, compared to the low viability of the cells, 38% (SD=5%, n=3), from the non-controlled case, the viability of the cells reaches 82% (SD=7%, n=3) with rate controlled cooling. Admittedly, more biological tests should be executed in the future meanwhile using various cell types; nevertheless, the preliminary results imply that the lower cooling rate maintained by our devices was able to minimize the occurrence of intracellular ice formation during the freezing process.

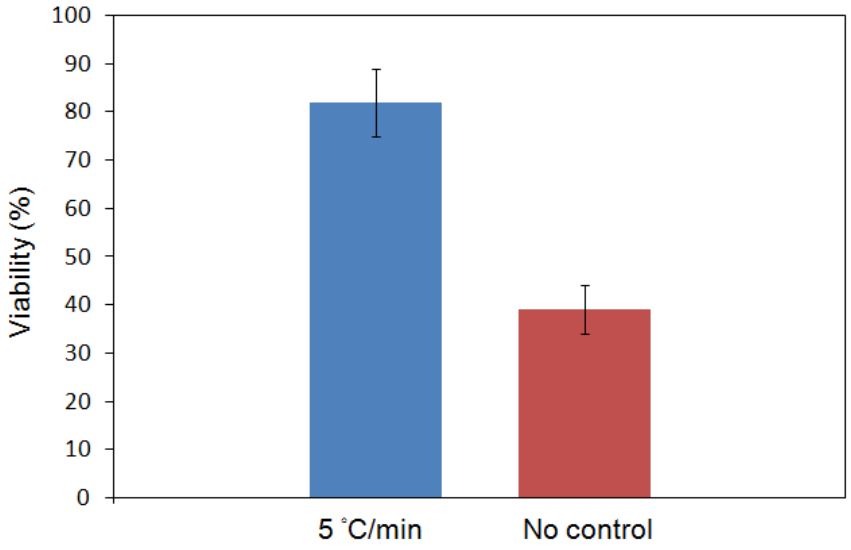

Figure 4.6. Cell viability and comparison between the cooling-rate control using the devices and no control using the cryogenic vials

4.4. Conclusion of the Work Presented in this Chapter

In this work, a proof-of-concept device toward a convenient tool for laboratory use in cryopreservation was developed. Our system consists of storage chambers, resistive heaters/temperature sensors on boards, and feedback-control instrumentation. The disposable storage chambers was fabricated and assembled, allowing the simple operations of wet processes. The copper serpentines were fabricated by the PCB technology and characterized to act as effective heating and temperature sensing elements. The closed-loop control instrumentation was realized to accurately monitor the temperature of the samples and automatically adjust them to follow desired cooling rates. The heat transfer model was built to examine spatial temperature profiles in the chamber. Preliminary biological tests were performed to show the further use of the proposed device in practice. In conclusion, compared with the prior arts for cryopreservation which range from the Styrofoam boxes, alcohol chambers, programmable freezers, to the on-chip devices, our system owns advanced features and acceptable performance that include industrial friendly manufacturing, user friendly operational process and experimental setup, accurate temperature monitoring, and rate controlled cooling. It is suggested that further investigation with respect to instrumentation will lead to a more powerful and efficient

multiplexing array using high-end control mechanism, such as a field-programmable gate array (FPGA). An industrial design for standardized manufacturing of the storage chambers, more biological tests, and a sophisticated user interface should also be considered before commercialization efforts. As a prototype that for the first time integrated multiple functions and processes into one device, the proposed work in this chapter fulfills the demand of a low-cost, simple and reliable rate controlled cooling system to serve as an applicable platform for optimized cryopreservation.

In this work, the heater boards and PDMS based chambers were made by automatic machining processes, showcasing industry-compatible standardized design and manufacturing processes. The array of heaters were fabricated using PCB technology for temperature control. The array of PDMS based chambers were fabricated by 3D printing and laser machining for sample loading. The developed array showcases the integration of multiple functional units to achieve complex design requirements. The heaters are connected to external instrumentation through solderable pin holes, showcasing reliable and convenient interconnections between devices and instrumentation. The miniaturized format of the prototyped device ensures its portability for POC bioprocessing. The experimental results indicate the outstanding performance of the rate controlled cooling to prior arts.

Chapter 5.

Future Development and Industrialization

5.1. Phases of Development

For the development of the proposed technology in all applications, three strategic phases can be considered: (1) proof of concept, (2) design for manufacturing and (3) commercialization. In the proof of concept phase, applications and their scientific mechanisms should be defined and tested. A prototyped device should also be developed afterwards. In the phase of design for manufacturing, the design and manufacturing processes should be optimized to ensure the feasibility of mass production. Specific operational protocols, system optimization and clinical tests should be completed for different applications. Lastly, in the phase of commercialization, business models and plans should be respectively established and executed.

In chapters 2-4, proof-of-concept and design for manufacturing have been applied to three example demonstrator systems where PCB technology is used to facilitate development. The scientific mechanism and problem solving of each technology was proven by experiments. New platforms, materials and methods were carried out to build prototypes and explore new design concepts and manufacturing for the future mass production of these devices. Preliminary operational protocols and instrumentation were also developed to work with the prototypes.

In this thesis, sample chambers made of polymers were simply attached onto the on-board devices to contain standstill liquids. However, multiplexed sample-reagent interactions and control may be required by other biosensing and bioprocessing applications. In the future, on-board microfluidics can be developed with the following three focuses: (1) microfluidic layouts for multiplexed purposes, (2) design of on-board microfluidic elements (e.g. valves and mixers) and (3) development of industry-compatible materials and methods. Three challenges may be encountered during the development as following: (1) cross contaminations between samples, (2) large off-chip support devices and (3) machining of microfluidic structures and bonding between them and boards.

Addressing cross contaminations between samples, 3D microfluidic channels are suggested to increase options for channel routing. Addressing large off-chip support devices, the configuration of microfluidic elements should be designed to ensure their actuating effectiveness with low power consumption. A search of multi-functional materials, which are photo-patternable, bio-compatible, and bondable to various types of substrate, is suggested to be carried out to address the integration of microfluidic structures and boards.

In summary, future work may include (1) exploring more applications based on the proposed technology; (2) realizing proposed design and manufacturing with industrialized approaches; (3) developing on-board microfluidics with complex networks and fluid handling elements for multiplexed biosensing and bioprocessing; (4) optimizing instrumentation in portable formats; (5) developing user interfaces; and (6) executing clinical or field tests. The overall plan proposed in this section serves as a preliminary guide for the future development of the proposed PCB-based technology.

5.2. Business Perspectives

Despite a pathway toward the practical use or commercialization of a POC product requiring valid scientific mechanism, reliable manufacturing, feasible operational protocols, and some miscellaneous items such as system optimization and clinical tests, a promising and rational business model is a significant indicator of whether these technical efforts will be successfully converted into sustainable opportunities. In this section, three brief business models are proposed for the proposed technology.

First, new biosensing or bioprocessing products may be established by technology owners who initiate ideas and design prototypes. The technology owners may choose to be original-brand-manufacturers (OBM) who build up a lab or production line and hire necessary personnel to work on well-rounded tasks such as research & development, design & manufacturing, marketing & sales. This model requires larger funding investments and administrative management.

Second, academic researchers or young entrepreneurs developing POC biosensing or bioprocessing using advanced PCB technology may find a simpler and less risky pathway by sending their finalized designs to original equipment manufacturers (OEM), in this case, PCB manufacturers, to fabricate or assemble parts for their products.

Third, an even simpler pathway may be offered by original design manufacturers (ODM) to idea owners or clients with specific and customized requirements about their applications. This model can be further divided into two steps whereby tasks are sent by clients to designers and designs are sent by designers to manufacturing sites.

The previous sections and chapters of this thesis are primarily written from a standpoint of academic researchers. On the other hand, based on the three business models, a standpoint of PCB manufacturers may imply an interesting vision on the use of advanced PCB technology in biosensing and bioprocessing applications. PCB manufacturing is originally one of the most important industry in the chain of electronics manufacturing, generating an estimated output value of 5.5 billion dollars in 2014 [70]. However, due to the globalization, currently the share of worldwide PCB market by North American PCB manufacturers is below 10% [70]. Perhaps the best way to break through

the North American disadvantage of higher manufacturing and labor costs is to find new applications and define new markets. The above mentioned three business models of the proposed technology may imply an opportunity for PCB manufacturers in North America.

Chapter 6.

Contributions of the Thesis

6.1. Contributions of the Thesis

The work presented in this thesis makes the following contributions to the field of point-of-care biosensing and bioprocessing devices and systems:

1. New manufacturing processes based on industrialized materials and methods have been developed for POC biosensing and bioprocessing applications to:

   - ensure the feasibility of future mass production by using PCB technology, which already has major infrastructure with automatic production lines used for many consumer products in electronic manufacturing industry and easily integrated with other manufactured equipment,

   - incorporate or fabricate multiple functional elements (e.g. pH sensor, microelectrodes, heater, thermometer, sample chamber) in 3D configurations utilizing the multilayer feature of PCB technology,

   - ensure reliable communication between the devices and external instrumentation through solderable pin holes that have already been thoroughly characterized by industry,

   - ensure the compactness of the devices with minimum feature sizes in the micro-scale (50 μm), overall device size in meso-scale (around 5 mm).

2. PCB technology as a new option and problem solving tool for academic researchers have been demonstrated to:

   - expand the functionality of their POC biosensing/bioprocessing devices,

   - facilitate the translation of these devices into practical products,

- achieve comparable performance to the bench-top standards.

3. Development of three demonstration devices that highlight key aspects of the PCB-based technology proposed in this thesis, each with their own application-specific results that further make contributions to their respective fields as facilitated by the PCB-based technology. These devices include:

   - pH-based rapid screening for glucose-6-phosphate dehydrogenase deficiency
   - electrochemical biosensor assay for quantitative polymerase chain reactions
   - on-board array for cooling rate controlled cryopreservation

4. In addition to the academic community, this thesis also indicates new applications and possibility for the industry of PCB manufacturing.

6.2. Publications resulting from the thesis work

The presented efforts in this thesis have been converted into the following publications:

1. "On-Board array for multiplexed semi-active cooling rate controlled cryopreservation of living cells", **H. Y. Tseng**, S. Malfesi, M. Rahbar, N. Tehranchi, J. Jones, B. L. Gray, *Journal of Medical and Biological Engineering,* Accepted (2015).

2. "Development of rapid screening for glucose-6-phosphate dehydrogenase deficiency prior to malaria treatment utilizing on-board pH-based electrochemical assay", **H. Y. Tseng**, S. Malfesi, J. Lum, B. L. Gray, *Measurement*, 73, 158-161 (2015).

3. "Development of an electrochemical biosensor array for q-PCR reaction utilizing three-metal PCB technology", **H. Y. Tseng**, V. Adamik, J. Parsons, S. Lan, S. Malfesi, J. Lum, L. Shannon, B. Gray, *Sensors and Actuators B*, 204, 459-466 (2014).

4. "On-Board array for multiplexed semi-active cooling rate controlled cryopreservation of living cells", **H. Y. Tseng**, S. Malfesi, N. Tehranchi, J. Jones, B. L. Gray, *The 37th Canadian Medical and Biological Engineering Conference*, Oral Presentation (May, 2014).

In addition, other relevant work contributed to by the thesis author includes:

1. "High aspect ratio magnetic nanocomposite polymer cilium" (Best Student Paper Award), M. Rahbar, **H. Y. Tseng**, B. L. Gray, Proceedings of SPIE Microfluidics, BioMEMS, and Medical Microsystems XII, 8976 (2014).

Conclusions

Micro electro mechanical systems (MEMS) techniques have been widely used by academic researchers to develop promising biosensing and bioprocessing applications on miniaturized silicon/glass chips of millimeters or centimeters in size. However, major challenges have been encountered by academic researchers using Bio-MEMS technology to translate their devices toward practical products. This thesis has investigated such integration problems at configuration and system levels. Addressing these challenges, this thesis presents the use of printed circuit board technology to facilitate the development of POC biosensing and bioprocessing with three demonstrators including enzyme assays, quantitative polymerase chain reactions and cooling-rate controlled cryopreservation. Recall that the goal of the thesis is to attain the following characteristics; each of these goals is accomplished as follows, which also reflects the stated technological objectives of the thesis:

- Industry-compatible standardized design and manufacturing processes

  Manufacturing processes for POC biosensing and bioprocessing applications have been developed based on the industrialized materials and methods of PCB technology to ensure the feasibility of future mass production.

- Integration/Fabrication of multiple functional units to achieve complex experimental conditions

  The multilayer feature of PCB technology has been utilized to fabricate or incorporate multiple functional elements for POC biosensing and bioprocessing in 3D configurations.

- Reliable and convenient interconnections between devices and instrumentation

  Reliable and convenient solder-able surface-mount or pin-hole interconnections between on-board devices and external instrumentation have been established.

- Miniaturized format for portable purposes

Manufacturing resolutions down to micro-scale have been achieved to ensure the compactness of devices

- Competitive performance of target biosensing and bioprocessing applications

  The performance of the target POC biosensing and bioprocessing applications has been successfully demonstrated and compared with bench-top standards.

- Possibility of being integrated with microfluidic platforms

  Sample chambers have been used in three demonstration devices. On-board microfluidics will be investigated in the future work.

Based on the work presented in this thesis, the future development plan and possible business opportunities of the proposed technology further expand the possibility of its future implementation and commercialization in the field of POC biosensing and bioprocessing.

References

[1] Whitesides GM. The origins and the future of microfluidics. *Nature* 2006;442:368–73.

[2] Janasek D, Franzke J, Manz A. Scaling and the design of miniaturized chemical-analysis systems. *Nature* 2006;442:374–80.

[3] MicroTAS 2014. http://www.microtas2014.org/ (Accessed February 22nd, 2015).

[4] IEEE-Sensors 2014. http://ieee-sensors2014.org/ (Accessed February 22nd, 2015).

[5] Transducers 2013. http://transducers-eurosensors2013.org (Accessed February 22nd, 2015).

[6] Chin C, Linder V, Sia S. Commercialization of microfluidic point-of-care diagnostic devices. *Lab Chip* 2012;12:2118-34.

[7] Sackmann EK, Fulton AL, Beebe DJ. The present and future role of microfluidics in biomedical research. *Nature 2014;*507:181-9.

[8] Becker H. Collective wisdom. *Lab Chip* 2010;10:1351-4.

[9] Li J, Wang Y, Dong E, Chen H. USB-driven microfluidic chips on printed circuit boards. *Lab Chip* 2013;14:860-4.

[10] Burdallo I, Jimenez-Jorquera C, Fernández-Sánchez C, Baldi A. Integration of microelectronic chips in microfluidic systems on printed circuit board. *J Micromech Microeng* 2012;22:10.

[11] Kontakisa K, Petropoulosa A, Kaltsasa G, Speliotisc T, Gogolidesa E. A novel microfluidic integration technology for PCB-based devices: Application to microflow sensing. *Microelectronic Engineering* 2009;86:1382-4.

[12] Marshall LA, Wu LL, Babikian S, Bachman M, Santiago JG. Integrated printed circuit board device for cell lysis and nucleic acid extraction. *Anal Chem 2012;*84:9640−5.

[13] Khandpur RS. Printed circuit boards: design, fabrication, assembly and testing, Tata-McGraw Hill. 2005.

[14] IEC-PCV Consumables & Equipment. http://www.ieccan.com/pcb.htm/ (Accessed March 15th, 2015).

[15] E. Beutler, Glucose-6-phosphate dehydrogenase deficiency: a historical perspective. *Blood* 2008;111:16-24.

[16] Cappellini MD, Fiorelli G. Glucose-6-phosphate dehydrogenase deficiency. *Lancet* 2008;371:64-74.

[17] Fanello CI, Karema C, Avellino P, Bancone G, Uwimana A, Lee SJ, d'Alessandro U, Modiano D. High risk of severe anaemia after chlorproguanil-dapsone+artesunate antimalarial treatment in patients with G6PD (A-) deficiency. *PLoS One* 2008;3:e4031.

[18] Nkhoma ET, Poole C, Vannappagari V, Hall SA, Beutler E. The global prevalence of glucose-6-phosphate dehydrogenase deficiency: a systematic review and meta-analysis. *Blood Cells Mol Dis* 2009;42:267-278.

[19] Glucose-6-phosphate dehydrogenase, in: Worthington Enzyme Manual. Worthington Biochemical Corporation. New Jersey. p13. 1972.

[20] Beutler E. Red Cell Metabolism: A Manual of Biochemical Methods. 3rd ed. Grune and Stratton. New York. 1984.

[21] Tinley KE, Loughlin AM, Jepson A, Barnett ED. Evaluation of a rapid qualitative enzyme chromatographic test for glucose-6-phosphate dehydrogenase deficiency. *Am J Trop Med Hyg* 2010;82:210-214.

[22] Kim S, Nguon C, Guillard B, Duong S, Chy S, Sum S, Nhem S, Bouchier C, Tichit M, Christophel E, Taylor WR, Baird JK, Menard D. Performance of the CareStart™ G6PD deficiency screening test, a point-of-care diagnostic for primaquine therapy screening. *PLoS One* 2011;6:e28357.

[23] Miao Y, Guan J, Chen J. Ion sensitive field effect transducer-based biosensors. *Biotechnology Advances* 2003;21:527-34.

[24] Dzyadevych SV, Soldatkin AP, El'skaya AV, Martelet C, Jaffrezic-Renault N. Enzyme biosensors based on ion-selective field-effect transistors. *Analytica Chimica Acta* 2006;568:248–58.

[25] Smith RL, Scott DC, An integrated sensor for electrochemical measurements. *IEEE Transactions on Biomedical Engineering, Special Issue on Biosensors. BME-33* 1986;2:83-90.

[26] Jamasb S, Collins SD, Smith RL. A physical model for drift in ISFET's. *Sens and Actuat B* 1998;B49:146-155.

[27] R. Mukhopadhyay, Microfluidics: On the Slope of Enlightenment. *Anal Chem* 2009;81:4169–4173.

[28] Wang K, Chen Y, Lei Y, Zhong G, Liu A, Zheng Y, Sun ZL, Lin X, Chen Y. Electrochemical method for monitoring the progress of polymerase chain reactions using Methylene blue as an indicator. *Microchim Acta 2013;*180:871-8.

[29] Won B, Shin S, Baek S, Jung Y, Li T, Shin S, Cho D, Lee S, Park H. Investigation of the signaling mechanism and verification of the performance of an electrochemical real-time PCR system based on the interaction of methylene blue with DNA. *Analyst* 2011;136:1573.

[30] Xu H, Gao S, Hou F. Electrochemical Behaviors of Methylene Blue on DNA Modified Gold Electrode. *Current Physical Chemistry* 2011;1:7-10.

[31] Luo X, Xuan F, Hsing IM. Real time electrochemical monitoring of PCR amplicons using electroactive hydrolysis probe. *Electrochemistry Communications* 2011;13:742-5.

[32] Kopp MU, Mello AJ, Manz A. Chemical amplification: continuous-flow PCR on a chip. *Science* 1998;280:1046-8.

[33] Kamamaka K, Saito M, Kondoh K, Hossain M, Koketsu R, Sasaki T, Nagatani N, Ikuta K, Tamiya E. Rapid detection for primary screening of influenza A virus: microfluidic RT-PCR chip and electrochemical DNA sensor. *Analyst* 2011;136:2064-8.

[34] Lee TMH, Carles MC, Hsing IM. Microfabricated PCR-electrochemical device for simultaneous DNA amplification and detection. *Lab Chip* 2003;3:100-105.

[35] Yeung SSW, Lee TMH, Hsing IM. Electrochemistry-Based Real-Time PCR on a Microchip. *Anal. Chem.,* 2008;80:363-8.

[36] Loncaric C, Tang Y, Ho C, Parameswaran MA, Yu H. A USB-based electrochemical biosensor prototype for point-of-care diagnosis. *Sensors and Actuators B* 2012;161:908-13.

[37] Ferreira H, Daniel D, Bertottib M, Richter E. A novel disposable electrochemical microcell: construction and characterization. *J. Braz. Chem. Soc.* 2008;19:1538-45.

[38] Prasek J, Trnkova L, Gablech I, Businova P, Drbohlavova J, Chomoucka J, Adam V, Kizek R, Hubalek J. Optimization of planar three-electrode systems for redox system detection. *Int. J. Electrochem. Sci.* 2012;7:1785-1801.

[39] Wu LL, Babikian S, Li GP, Bachman M. Microfluidic printed circuit boards. *IEEE 61st Electronic Components and Technology Conference* 2011*;*1576-81.

[40] Gong J, Kim CJ. Direct-referencing two-dimensional-array digital microfluidics using multilayer printed circuit board. *J Microelectromech Syst* 2008;17:257-264.

[41] Paunovic M. Electroless Plating of Copper, in: Schlesinger M and Paunovic M (Eds.). *Modern Electroplating*, fifth ed. J. Wiley and Sons Inc. Hoboken, NJ. 2010;433-446.

[42] Schlesinger M. Electroless Deposition of Nickel, in: Schlesinger M and Paunovic M (Eds.), *Modern Electroplating*, fifth ed. J. Wiley and Sons Inc. Hoboken, NJ. 2010;447-458.

[43] Okinaka Y, Kato M. Electroless Deposition of Gold, in: Schlesinger M and Paunovic M (Eds.), *Modern Electroplating*, fifth ed. J. Wiley and Sons Inc. Hoboken, NJ. 2010;483-498.

[44] Schlesinger M, Electroless and Electrodeposition of Silver, in: Schlesinger M and Paunovic (Eds.), *Modern Electroplating*, fifth ed. J. Wiley and Sons Inc. Hoboken, NJ. 2010;131-138.

[45] Radoeva M, Radoev B. Ohm resistivity of electroless copper layers as a function of their thickness. *J Material Sci* 1995;30:2215-9.

[46] Kinkead B, Drunen J, Paul M, Dowling K, Jerkiewicz G, Gates B. Platinum ordered porous electrodes: developing a platform for fundamental electrochemical characterization. *Electrocatalysis* 2013;4:178-86.

[47] Kissinger P, Heineman W. Laboratory Techniques in *Electroanalytical Chemistry*. Dekker. New York. 1983.

[48] Zhu L, Zhao R, Wang K, Xiang H, Shang Z, Sun W. Electrochemical Behaviors of Methylene Blue on DNA Modified Electrode and Its Application to the Detection of PCR Product from NOS Sequence. *Sensors* 2008;8:5649-60.

[49] Yang W, Ozsoz M, Hibbert DB, Gooding JJ. Evidence for the Direct Interaction Between Methylene Blue and Guanine Bases Using DNA-Modified Carbon Paste Electrodes. *Electroanalysis* 2002;14:1299-302.

[50] Adams MD, Celniker SE, Holt RA. The genome sequence of Drosophila melanogaster. *Science* 2000;287:2185-95.

[51] Benson DA, Karsch-Mizrachi I, Lipman DJ, Ostell J, Sayers EW. *GenBank. Nucleic Acids Res* 2011;39:D32–37.

[52] Ikeuchi H, Kanakubo M, Watanabe Y, Naito T, Sato GP. Chronoamperometric determination of diffusion coefficients under microgravity conditions. *J. Electroanalytical Chemistry* 2004;562:105-10.

[53] Charles JH. Cryopreservation of Human Stem Cells for Clinical Application: A Review. *Transfus Med Hemother* 2011;38:107-23.

[54] Toner M, Cravalho E, Stachecki J. Nonequilibrium freezing of one-cell mouse embryos membrane integrity and development potential. *Biophys J* 1993;64:1908-21.

[55] Mazur P. Freezing of Living Cells – Mechanisms and Implications. *Am. J. Physiol.* 1984;14:C125-42.

[56] Bank H, Mazur P. Visualization of freezing damage. *J Cell Biol* 1973;57:729-42.

[57] Toner M, Cravalho E, Karel M. Thermodynamics and Kinetics of Intracellular Ice Formation during Freezing of Biological Cells. *J. Appl. Phys.* 1990;67:1582-93.

[58] Lovelock J. The denaturation of lipid-protein complexes as a cause of damage by freezing. *Proc. Roy. Soc. London B.* 1957;147:427-34.

[59] Mazur P. Slow-freezing injury in mammalian cells, in: Elliott K and Whelan J (Ed.), *The freezing of mammalian embryos*. Elsevier. Amsterdam. 1977;19-42.

[60] Mazur P, Leibo S, Chu E. A two-factor hypothesis of freezing injury. *Exp. Cell Res*. 1972;71:345-55.

[61] Tseng HY, Sun S, Shu Z, Ding W, Reems J, Gao D. A microfluidic study of membrane transport properties of human megakaryocytes to Water and DMSO. *Biopreservation and Biobanking* 2011;9:355-62.

[62] Shu Z, Kang X, Chen H, Zhou X, Putteman J, Yadock D, Heimfeld S, Gao D. Development of a reliable, low-cost, controlled cooling rate instrument for the cryopreservation of hematopoietic stem cells. *Cytotherapy* 2010;12:161-9.

[63] Chen HH, Purtteman JP, Heimfeld S, Folch A, Gao D. Development of a microfluidic device for determination of cell osmotic behavior and membrane transport properties. *Cryobiol* 2007;55:200-9.

[64] Chen HH, Shen H, Heimfeld S, Tran KK, Reems J, Folch A, Gao D. A microfluidic study of mouse dendritic cell membrane transport properties of water and cryoprotectants. *Intl. J. Heat & Mass Transfer* 2008;51:5687-94.

[65] Kuwayama M, Leibo S. Cryopreservation of Human Embryos and Oocytes. *J Mamm Ova Res* 2010;27:79-86.

[66] Sputtek A. Cryopreservation of Red Blood Cells and Platelets. *Methods Mol Bio* 2007;368:283-301.

[67] Li S, Liu W, Lin L. On-Chip Cryopreservation of Living Cells. *JALA* 2010;15:99-106.

[68] Wescott T. PID without a PhD. *Embedded System Programming*. October, 2000;86-108.

[69] Incropera F, Dewitt DP, Bergman TL, Lavine AS. *Introduction to Heat Transfer*. Wiley. New Jersey. 2011.

[70] China Times. http://www.chinatimes.com/newspapers/20140723000149-260210 (Accessed May, 2015).

Appendix A.

Arduino Code

PID Controller for the Temperature Control Program

```
const int MAXREAD = 1023;        //max value for adc
const int debuglevel = 1;        //used sto set the
const int numIn = 2;             // number of adc inputs
//varuables used for the digital low pass so sensor anomolies will not have much weight
const int buffersize = 10;
int bufferIndex = 0;
float readbuffer[numIn][buffersize];
float total[numIn];
//used to set the frequency of serial writes
const int maxcount = 100;
int count = 0;
//pin used to set voltage across the heater
const int pwmPin = 9;
int pwm = 0;
//constants used to calculate the temerature
const float ialpha = 30; //inverse alpha typically 250
const float rh = 7.66;   //heaters resistance at T0
const float rb = 4.5;    //bottem resistance assumed to be constant
const float ialpharr= ialpha*rb/rh; //IALPHA100*RB/RH
const float T0 = -50;    //starting temp
//constants used to set the pid contorller
const float kp = 100;    //proportional  larger makes it heat faster
const float kd = 1;      //derivative    allows for larger kp with less
const float ki = 2;      //integral      to avoid steady state error
```

```
const float MAX_ERROR_SUM = 200;        //the integral part from going too nuts
float errorSum = 0;
float lastTemp = T0;
const int mode = 0;           // 0 = const, 1 = slope, 2 = cycle
float target = -200;          // target for constant mode
const float degPerMin = 10;   // desired rate for slope mode
const int targetSize = 3;      //targets for cycle
const float targets[targetSize] = {52, 73, 95};
const long holdTime = 30000;   //hold time for time in cycle
int targetIndex = -1;
long startTime = 0;
int newTarget = 1;
// setup is run first and initializes neceary parts
void setup()
{
  Serial.begin(9600);
  pinMode(pwmPin, OUTPUT);
    for(int j = 0; j < numIn; j++)
  {
    total[j]=0;
    for(int i = 0; i < buffersize; i ++)
    {
      readbuffer[j][i]=0;
    }
  }
}
// prints variable over serial at a lower rate and if the debug level is set low
void printn(char* name, float value, int debugflag)
{
```

```
  if(count >= maxcount && debuglevel >= debugflag)
  {
    Serial.print(name);
    Serial.print("  ");
    Serial.print(value);
    Serial.print("    ");
  }
}
//Reads the analog input values and averages them the last buffersize reads
float readAverageAnalogRatio()
{
  float sensorValue[numIn];
  //sets the pwn pin high before read so that the transister will be on
  digitalWrite(pwmPin, HIGH);
  delay(2); // wait to make sure it is on before the read
  sensorValue[0] = (float) (MAXREAD - analogRead(A0));
  sensorValue[1] = (float) analogRead(A1);
  analogWrite(pwmPin, pwm);
  // maps the sensor values to the voltage value
  printn("vh",((float) map(sensorValue[0], 0, 1023, 0, 500))/100, 1);
  printn("vb",((float) map(sensorValue[1], 0, 1023, 0, 500))/100, 1);
    // should not be zero. this indicates a failed read and should be disregarded
  if(sensorValue[0] > 0 && sensorValue[1] > 0)
  {
    for(int i = 0; i < numIn; i++)
    {
      //instead of adding all of the buffer every time, we just remove value from the last total
      total[i] = total[i] - readbuffer[i][bufferIndex];
      readbuffer[i][bufferIndex] = sensorValue[i];
```

```
      total[i] = total[i] + sensorValue[i];
      //debug for buffered values
      printn("\n",0, 3);
      for(int j = 0; j < buffersize; j++)
      {
        printn("b", readbuffer[i][j], 3);
      }
      printn("\n",0, 3);
        }
    //resets buffer index when its out of range to create a circuilar buffer
    bufferIndex = (bufferIndex >= buffersize - 1) ? 0 : bufferIndex + 1;
  }
     printn("t0",total[0]/buffersize, 3);
   printn("t1",total[1]/buffersize, 3);
    float ratio = (total[0])/(total[1]);
  return ratio; // ratio is all thats needed for later
}
//reads and does pid control
void Control()
{
  float ratio = readAverageAnalogRatio();
  float temp = (ialpharr * ratio) - ialpha + T0;
  float error = target - temp;
    //if you are in cycle mode and have made it to the next target start timer
  if(mode == 2 && error < 2 && newTarget > 0)
  {
    startTime = millis();
    newTarget = 0;
  }
```

```
    errorSum = constrain(errorSum + error, -MAX_ERROR_SUM, MAX_ERROR_SUM);
    float pTerm = kp * error;
  float iTerm = ki * errorSum;
  float dTerm = kd * (temp - lastTemp);
    lastTemp = temp;
  int nextVal = (int) (pTerm + iTerm - dTerm);
  pwm =  constrain(nextVal, 0, 255);
    analogWrite(pwmPin, pwm);
  printn("temp", temp, 0);
  printn("error", error, 1);
  printn("errorSum", errorSum, 2);
  printn("pwm", pwm, 1);
    //this delay makes it so the read (which sets the pwm pin high for 100 ms)
  //isnt run too often.
  delay(10);
}
// calcualtes the target value given the mode and current time
float NextTarget()
{
  float nexttarget = target;
  switch(mode)
  {
  case 1: // slope mode
    nexttarget = degPerMin * ((float) (millis() - startTime)) / 60000.0 + T0;
    break;
  case 2: //cycle mode
    printn("time", ((float)(millis() - startTime))/1000.0, 1);
    if((millis() - startTime) > holdTime && newTarget < 1)
    {
```

```
      targetIndex = (targetIndex + 1 < targetSize) ? targetIndex + 1 : 0;
      nexttarget = targets[targetIndex];
      newTarget = 1;
      startTime = millis();
    }
    break;
  default:
  case 0: // constant mode (do nothing)
  break;
 }
 printn("target", nexttarget, 1);
 return nexttarget;
}
//main loop, run constantly
//while(1)
void loop()
{
  target = NextTarget();
  Control();
   //increase loopcount and reset when necessary
  count++;
  if(count > maxcount)
  {
    count = 0;
    Serial.write('\n');
  }
}
```